NJC

ROYAL SOCIETY OF CHEMISTRY

PAPER

View Article Online
View Journal | View Issue

Cite this: *New J. Chem.*, 2021, 45, 881

[1,2,4]Triazolo[4,3-*a*]quinoxaline and [1,2,4]triazolo[4,3-*a*]quinoxaline-1-thiol-derived DNA intercalators: design, synthesis, molecular docking, *in silico* ADMET profiles and anti-proliferative evaluations†

Khaled El-Adl, *[ab] Abdel-Ghany A. El-Helby,[a] Helmy Sakr[a] and Alaa Elwan[a]

Received 15th June 2020,
Accepted 29th November 2020

DOI: 10.1039/d0nj02990d

rsc.li/njc

In view of their DNA intercalation activities as anticancer agents, 17 novel [1,2,4]triazolo[4,3-*a*]quinoxaline derivatives have been designed, synthesized and evaluated against HepG2, HCT-116 and MCF-7 cells. Molecular docking studies were performed to investigate the binding modes of the proposed compounds with the DNA active site. The data obtained from biological testing highly correlated with those obtained from the molecular modeling studies. MCF-7 was found to be the most sensitive cell line to the influence of the new derivatives. In particular, compound **12$_d$** was found to be the most potent derivative of all the tested compounds against the three HepG2, HCT116 and MCF-7 cancer cell lines, with IC_{50} = 22.08 ± 2.1, 27.13 ± 2.2 and 17.12 ± 1.5 μM, respectively. Although this compound displayed nearly one third of the activity of doxorubicin (IC_{50} = 7.94 ± 0.6, 8.07 ± 0.8 and 6.75 ± 0.4 μM, respectively), it may be useful as a template for future design, optimization, and investigation to produce more potent anticancer analogs. Compounds **12$_a$**, **10$_c$** and **10$_d$** displayed very good anticancer activities against the three HepG2, HCT116 and MCF-7 cancer cell lines, with IC_{50} = 31.40 ± 2.8, 28.81 ± 2.4 and 19.72 ± 1.5 μM for **12$_a$**, 33.41 ± 2.9, 29.96 ± 2.5 and 24.78 ± 1.9 μM for **10$_c$**, and 37.55 ± 3.3, 30.22 ± 2.6 and 25.53 ± 2.0 μM for **10$_d$**. The most active derivatives, **10$_c$**, **10$_d$**, **10$_h$**, **12$_a$**, **12$_b$** and **12$_d$**, were evaluated for their DNA binding activities. Compound **12$_d$** displayed the highest binding affinity. This compound potently intercalates DNA at a decreased IC_{50} value (35.33 ± 1.8 μM), which is nearly equipotent to that of doxorubicin (31.27 ± 1.8 μM). Compounds **12$_a$** and **10$_c$** exhibited good DNA-binding affinities, with IC_{50} values of 39.35 ± 3.9 and 42.35 ± 3.9 μM, respectively. Finally, compounds **10$_d$**, **10$_h$** and **12$_b$** showed moderate DNA-binding affinities, with IC_{50} values of 50.35 ± 3.9, 57.08 ± 3.3 and 59.35 ± 3.2 μM, respectively.

1. Introduction

DNA plays an essential role in a wide diversity of cellular processes and acts as a fundamental target for treating hallmark genetic diseases such as cancer.[1] The most important group of compounds that interact reversibly with the DNA double helix are intercalators.[2] Many anticancer drugs that interact with DNA through intercalation are in clinical use.[2,3] Intercalation is a process in which the intercalating molecule is transferred from an aqueous environment to the hydrophobic space between two adjacent DNA base pairs.[3,4] Extensive research over the last four decades has focused on the effects of small organic compounds that non-covalently bind to nucleic acids.[5] These interactions are known to disrupt replication and/or transcription, which culminates in cellular death. Accordingly, DNA-binding compounds have potential applications as anticancer agents. Small molecules may bind non-covalently to DNA through intercalation between nucleobase pairs, major or minor groove binding and electrostatic interactions.[6] The planar aromatic portions of molecules (known as chromophores) are inserted between adjacent base pairs of the DNA helix perpendicularly to its axis, forming strong non-covalent interactions with DNA bases.[7,8] This complex between the drug and DNA deforms and uncoils the DNA;[7] also, the structural changes induced in DNA by intercalation lead to interference with

[a] *Pharmaceutical Chemistry Department, Faculty of Pharmacy, Al-Azhar University, Cairo, Egypt. E-mail: eladlkhaled74@yahoo.com, eladlkhaled74@azhar.edu.eg, khaled.eladl@hu.edu.eg*

[b] *Pharmaceutical Chemistry Department, Faculty of Pharmacy, Heliopolis University for Sustainable Development, Cairo, Egypt*

† Electronic supplementary information (ESI) available. See DOI: 10.1039/d0nj02990d

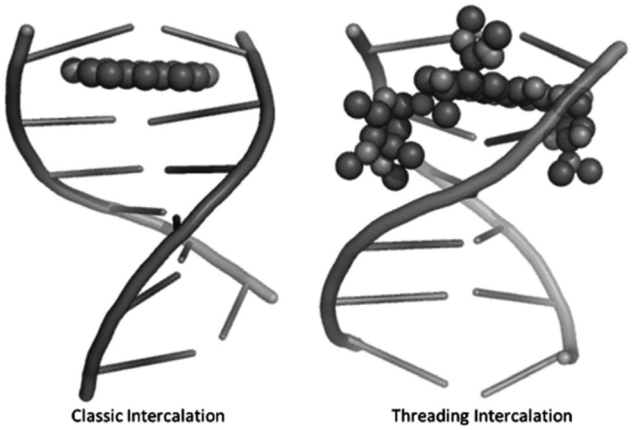

Fig. 1 Cartoon representations of the classical and threading modes of drug intercalation with DNA.

recognition and function of DNA-associated proteins or enzymes involved in replication, transcription, and DNA repair systems, leading to failure of these processes.[7]

There are two types of intercalators: classic/mono-intercalators and threading intercalators.[1] The presence of two groove-binding side chains, as in the case of nogalamycin **I**, which contains two sugar moieties at both ends of its chromophore, leads to a special type of interaction with DNA called threading intercalation, in which one sugar unit is oriented to the minor groove and the other to the major groove[7] (Fig. 1).

Many DNA intercalators are either being used already as anticancer drugs or are still in clinical trials (*e.g.*, nogalamycin **I**,[9] doxorubicin **II**,[10] and amsacrine **III**[11]) (Fig. 2).

The quinoxaline nucleus is the backbone of many DNA intercalators.[12–15] The discovery and development of new

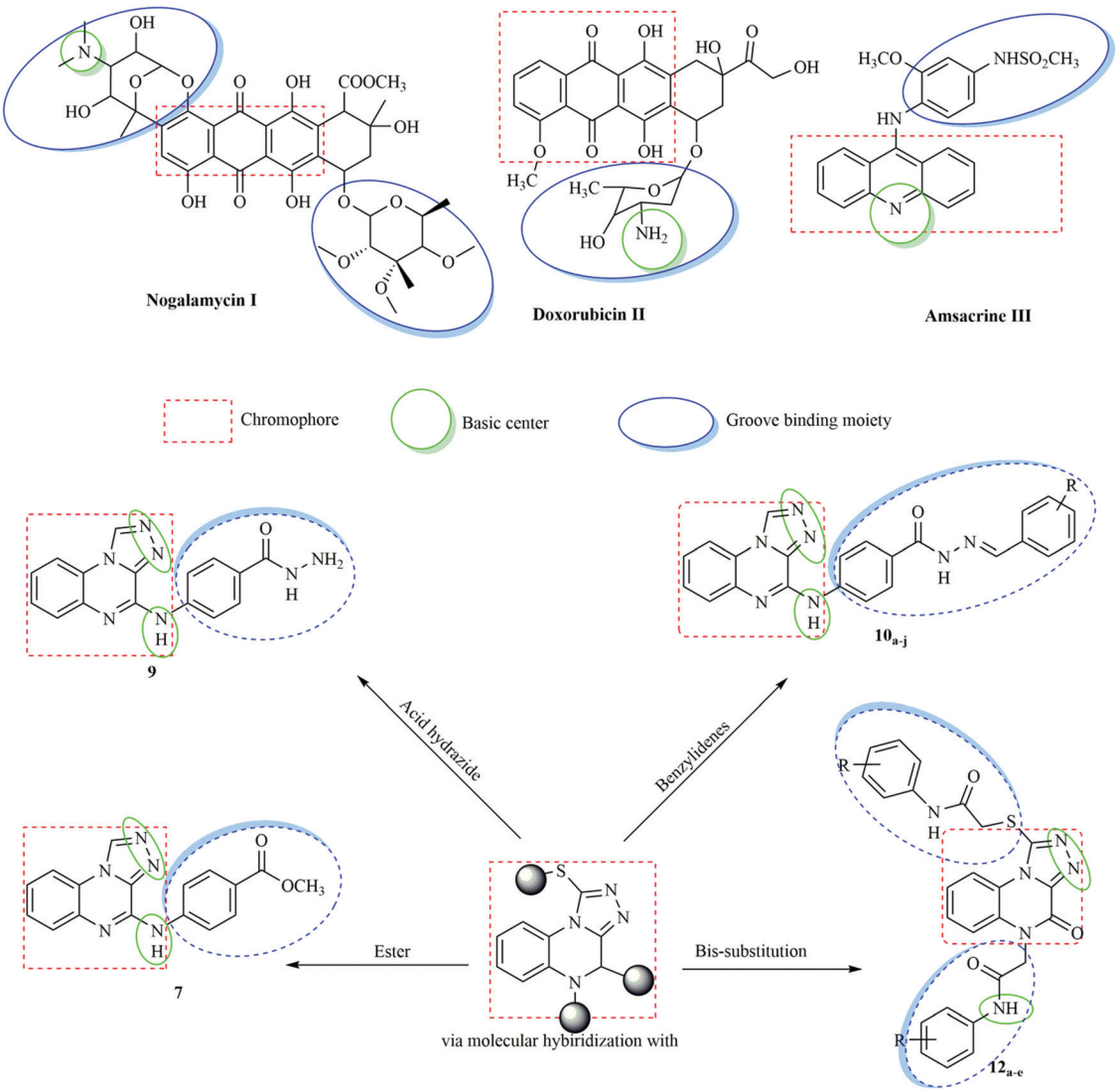

Fig. 2 Basic pharmacophoric features of reported DNA intercalators and our derivatives.

therapeutic DNA intercalators for the treatment of cancer is considered to be one of the most important targets in the field of medicinal chemistry.[16] Quinoxaline analogues demonstrate excellent anticancer activities through DNA intercalation; for instance, echinomycin **VI**, a natural DNA intercalator, showed potent activities in phase I and II trials against a wide array of cancers.[17] Moreover, N^3-(3-(dimethylamino)propyl)-N^2-(4-methoxybenzyl)-6-nitroquinoxaline-2,3-diamine **VII** is of current interest in view of its binding to DNA.[18]

On the other hand, quinoxaline derivatives have been reported to have different cellular-based anticancer mechanisms. These derivatives were reported to have anticancer activity through EGFR-TK inhibition.[19] Moreover, [1,2,4]triazolo[4,3-*a*] quinoxaline derivatives were reported as potent anticancer agents with dual EGFR kinase and tubulin polymerization inhibitory effects.[20] Furthermore, [1,2,4]triazolo[4,3-*a*]quinoxaline derivatives were reported as efficient adenosine A2B antagonists.[21,22]

Based on these earlier findings, and in continuation of our previous research in the design and synthesis of new anticancer agents,[23–29] especially DNA intercalators,[12] we report the design, synthesis, DNA binding examination and docking studies of a new series of quinoxaline derivatives as DNA intercalators. In general, the designed compounds were synthesized and evaluated for their *in vitro* anti-proliferative activities against three human tumor cell lines, namely, hepatocellular carcinoma (HCC) type (HepG2), human colorectal carcinoma-116 (HCT-116) and breast cancer (Michigan Cancer Foundation-7 (MCF-7)). The results prompted us to carry out further examinations to obtain deep insight into the mechanisms of action of the synthesized compounds.

The most cytotoxic agents were further evaluated to assess their binding affinities against DNA through DNA/methyl green assays. Moreover, molecular docking was carried out to examine the binding patterns of the compounds with the prospective target DNA active site (PDB-code: 4G0U).

1.1. Rationale and structure-based design

The rationale of our molecular design depended on the generation of a planar aromatic system containing the triazolo [4,3-*a*]quinoxaline scaffold (chromophore) with one or two groove-binding side chains. The synthesis of the title compounds was carried out by two pathways. The first pathway involves molecular hybridization of the quinoxaline nucleus with a 1,2,4-triazole moiety to produce a [1,2,4]triazolo [4,3-*a*]quinoxaline scaffold (chromophore) which is substituted at position 4 with different moieties, such as ester, acid hydrazide benzylidene, ketone, chalcone and/or pyrazole derivatives, as a single groove-binding side chain. These compounds were designed as classical DNA intercalators.

The second pathway was performed through molecular hybridization of the quinoxaline nucleus with the 1,2,4-triazole-3-thiol moiety to produce a [1,2,4]triazolo[4,3-*a*]quinoxaline-1-thiol scaffold (chromophore) substituted at both positions 1 and 5 with different acetanilides as two groove-binding side chains. These compounds were designed as threading DNA intercalators.

The choice of the different substituents was based on their relatively high lipophilicity, with the aim to pass through the nuclear membranes and achieve strong DNA intercalation. Moreover, the variability of the substitutions enabled us to study the structure–activity relationships of the final compounds.

All compounds were designed to comprise the main pharmacophoric features of DNA intercalators; the planar polyaromatic system (chromophore) was represented by the quinoxaline nucleus and its fused triazole ring intercalating the base pairs of the DNA. In addition, all of the designed compounds include basic nitrogen atoms that may be protonated at physiological pH to form cationic centers that increase the affinity and selectivity of these compounds; finally, all the compounds mainly contain one or two side chains (Fig. 2), exhibiting different antitumor activities. These side chains bind to the minor groove and/or the major groove, increasing the DNA binding affinity.

2. Results and discussion

2.1. Chemistry

For the synthesis of the target compounds, the sequence of the reactions is illustrated in Schemes 1–3. *o*-Phenylenediamine **1** was reacted with oxalic acid **2** in the presence of 4 N HCl to afford 2,3-(1*H*,4*H*)-quinoxalinedione **3**.[13,30] The latter was treated with thionyl chloride to afford 2,3-dichloroquinoxaline **4**,[13,30] which underwent reaction with hydrazine hydrate with continuous stirring at room temperature to produce 2-chloro-3-hydrazinylquinoxaline **5**.[13] Cyclization of **5** with triethylorthoformate resulted in 4-chloro[1,2,4]triazolo[4,3-*a*]quinoxaline **6**.[13] Heating of **6** with methyl 4-aminobenzoate in acetonitrile afforded the corresponding methyl ester **7**. On the other hand, cyclization of 2-chloro-3-hydrazinylquinoxaline **5** with CS_2 in the presence of KOH in absolute ethanol afforded the corresponding 4-chloro-[1,2,4]triazolo[4,3-*a*]quinoxaline-1-thiol **8**[31] (Scheme 1).

The methyl ester **7** was treated with hydrazine hydrate to obtain the corresponding acid hydrazide **9**, which was reacted with the appropriate benzaldehyde derivatives to afford the corresponding Schiff bases $\mathbf{10_{a–j}}$, respectively (Scheme 2).

Furthermore, heating of **8** with alcoholic potassium hydroxide unfortunately afforded the dipotassium salt **11** instead of the targeted potassium 4-chloro-[1,2,4]triazolo[4,3-*a*]quinoxaline-1-thiolate **13**, which may be due to air oxidation under the reaction conditions. The obtained dipotassium salt **11** was reacted with the appropriate chloroacetanilide derivative to afford the corresponding 1,5 derivatives $\mathbf{12_{a–e}}$, respectively (Scheme 3). The ^{1}H NMR spectra exhibited the appearance of two singlet peaks at about 4.34–4.56 δ ppm for the two introduced CH_2 groups, increased the integration of the aromatic protons and also resulted in the presence of two singlet peaks for the two amidic NH groups. Also, the mass spectroscopic chart for compound $\mathbf{12_a}$ supported the presence of its molecular ion peak at 484. The reaction of 4-chloro-[1,2,4]triazolo

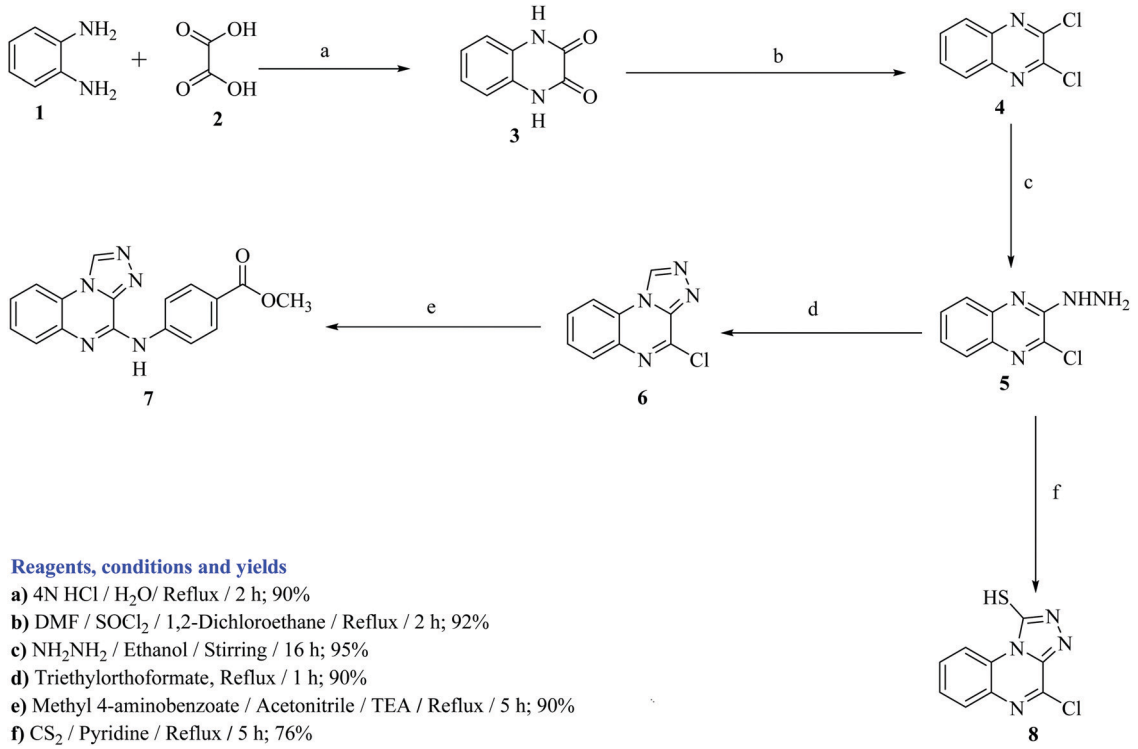

Reagents, conditions and yields

a) 4N HCl / H_2O/ Reflux / 2 h; 90%
b) DMF / $SOCl_2$ / 1,2-Dichloroethane / Reflux / 2 h; 92%
c) NH_2NH_2 / Ethanol / Stirring / 16 h; 95%
d) Triethylorthoformate, Reflux / 1 h; 90%
e) Methyl 4-aminobenzoate / Acetonitrile / TEA / Reflux / 5 h; 90%
f) CS_2 / Pyridine / Reflux / 5 h; 76%

Scheme 1 Synthetic route for the preparation of the target compounds **3–8**.

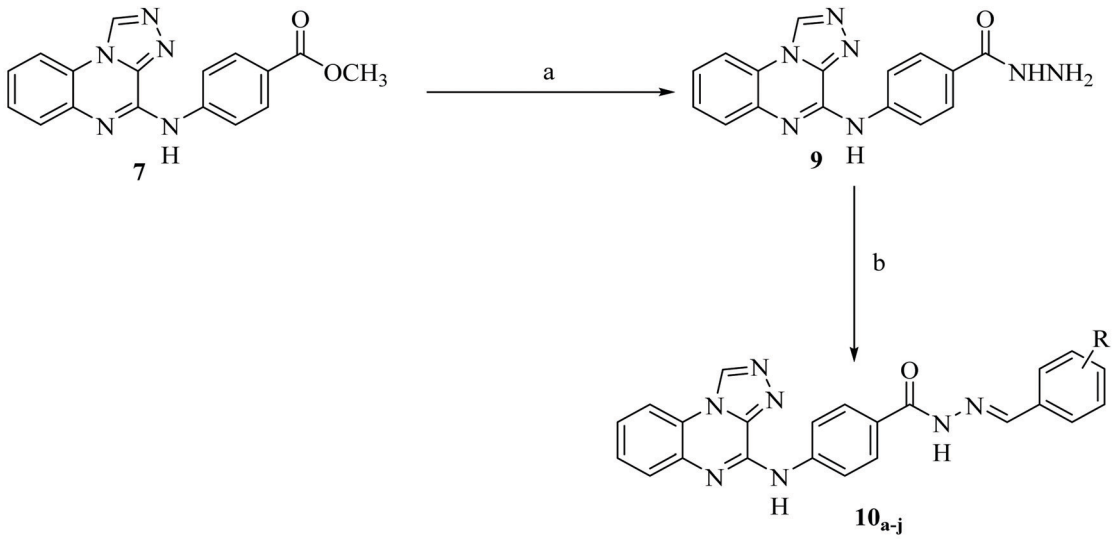

Reagents, conditions and yields

a) NH_2NH_2 / Ethanol / Reflux / 8 h; 80%
b) ArCHO/Ethanol / AcOH/ Reflux / 4 h; 80-95%

a) R = H
b) R = 2-Cl
c) R = 4-Cl
d) R = 4-F
e) R = 2,6-$(Cl)_2$
f) R = 4-OH
g) R = 2-OCH_3
h) R = 4-OCH_3
i) R = 3-NO_2
j) R = 4-NO_2

Scheme 2 Synthetic route for the preparation of the target compounds **9–10$_{a–j}$**.

[4,3-*a*]quinoxaline-1-thiol **6** with alcoholic potassium hydroxide was designed to produce the targeted potassium 4-chloro-[1,2,4]triazolo[4,3-*a*]quinoxaline-1-thiolate **13**. This potassium salt was designed to be reacted with the appropriate chloroacetanilide derivatives to furnish the targeted corresponding derivatives **14**, respectively. Furthermore, the derivatives **14$_{a–e}$** were designed to react with different aromatic amines to obtain diversity of compounds **15**. These reactions were

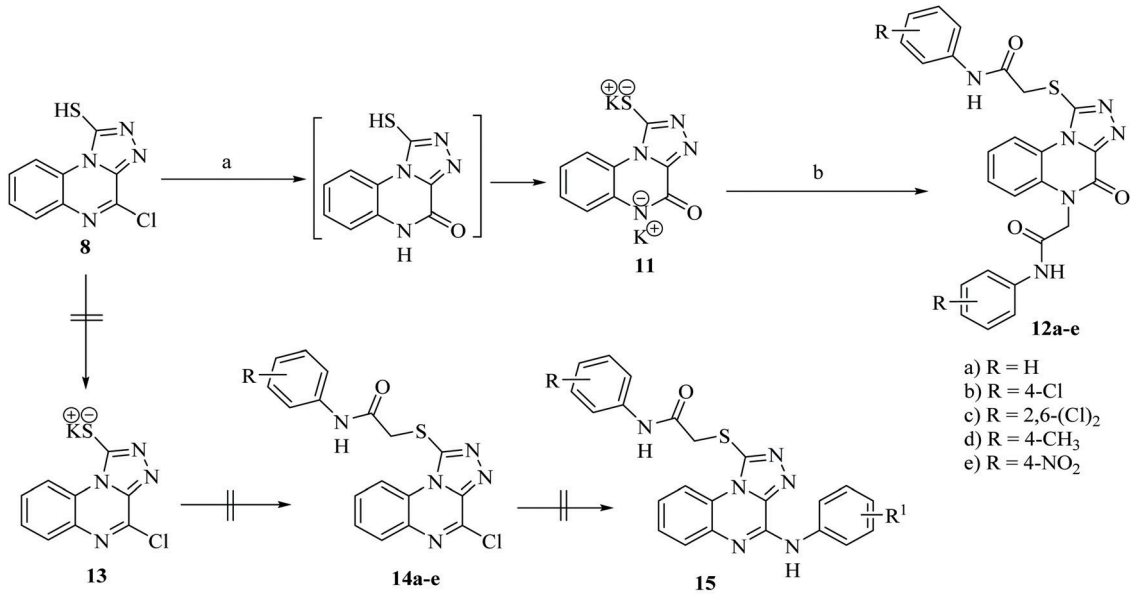

Scheme 3 Synthetic route for the preparation of the target compounds $\mathbf{12_{a-e}}$.

designed to obtain different substitutions at position 1 ($\mathbf{14_{a-e}}$) and also to combine the substitutions at positions 1 and 4 (**13**) in order to study the effects of these substitutions at different positions. Moreover, the designed reactions afforded a diversity of compounds to study the effects of the combinations of the two substitutions at two positions in the same compound and determine the structure activity relationships (SARs) of these derivatives. In fact, the data proved that the obtained $\mathbf{12_{a-e}}$ derivatives were disubstituted at positions 1 and 5, and the SARs were obtained for these compounds.

2.2. Docking studies

All the synthesized compounds were evaluated for their DNA binding affinity with the aid of molecular docking studies using Molsoft software. The 3D crystal structure of DNA was downloaded from the Protein Data Bank using the PDB ID of 4G0U.[32] The binding free energies (ΔG) are presented in Table 1. All the studied ligands have similar positions and orientations inside the DNA binding site.

Table 1 The calculated free energies of binding (ΔG in kcal mol^{-1}) of the ligands

Compound	ΔG [kcal mol^{-1}]	Compound	ΔG [kcal mol^{-1}]
7	−88.30	$\mathbf{10_h}$	−88.33
9	−80.92	$\mathbf{10_i}$	−79.05
$\mathbf{10_a}$	−80.50	$\mathbf{10_j}$	−80.06
$\mathbf{10_b}$	−80.44	$\mathbf{12_a}$	−104.45
$\mathbf{10_c}$	−89.88	$\mathbf{12_b}$	−88.30
$\mathbf{10_d}$	−88.50	$\mathbf{12_c}$	−79.11
$\mathbf{10_e}$	−80.01	$\mathbf{12_d}$	−105.42
$\mathbf{10_f}$	−79.16	$\mathbf{12_e}$	−79.08
$\mathbf{10_g}$	−79.14	Doxorubicin	−100.31

The proposed binding mode of doxorubicin revealed an affinity value of −100.31 kcal mol^{-1} and ten H-bonds. The planar aromatic system occupied the hydrophobic pocket formed by Arginine945, Asparagine882, Lucine880, Glutamate870, Alanine869, Glycine868, Asparagine867, Asparagine795, Glutamine789, Asparagine786, Glutamine742, Lysine739, Phenyalanine738 and Glycine737. It formed five H-bonds with the key amino acids in the active site (one H-bond with Asparagine786, two H-bonds with Asparagine795, one H bond with Arginine945, and one H-bond with Asparagine867). It also stacked between the diphosphate cytidines (Dc3, Dc4 and Dc8), diphosphate guanosines (Dg5 and Dg13) and adenine monophosphate 6 (Da6). The sugar moiety was oriented into the minor groove of the DNA and stabilized by the formation of five H-bonds with the key amino acids (two H-bonds with Arginine945, one H-bond with Leucine880 and two H-bonds with Asparagine882) (Fig. 3).

The proposed binding mode of $\mathbf{12_d}$ exhibited an affinity value of −105.42 kcal mol^{-1} and twelve H-bonds. The planar aromatic system occupied the hydrophobic pocket formed by Arginine945, Tyrosine908, Asparagine882, Glutamate870, Alanine869, Glycine868, Asparagine867, Asparagine798, Asparagine795, Glutamine789, Leucine787 and Asparagine786. It formed eight H-bonds with the key amino acid Arginine945. It also stacked between the diphosphate cytidines (Dc3, Dc4, Dc1 and Dc19) and diphosphate guanosines (Dg2, Dg5 and Dg13). The two substituted arms were oriented into the minor and major grooves of the DNA and were stabilized by the formation of four H-bonds with the key amino acids (one H-bond with Tyrosine908, one H-bond with Glutamine789 and two H-bond

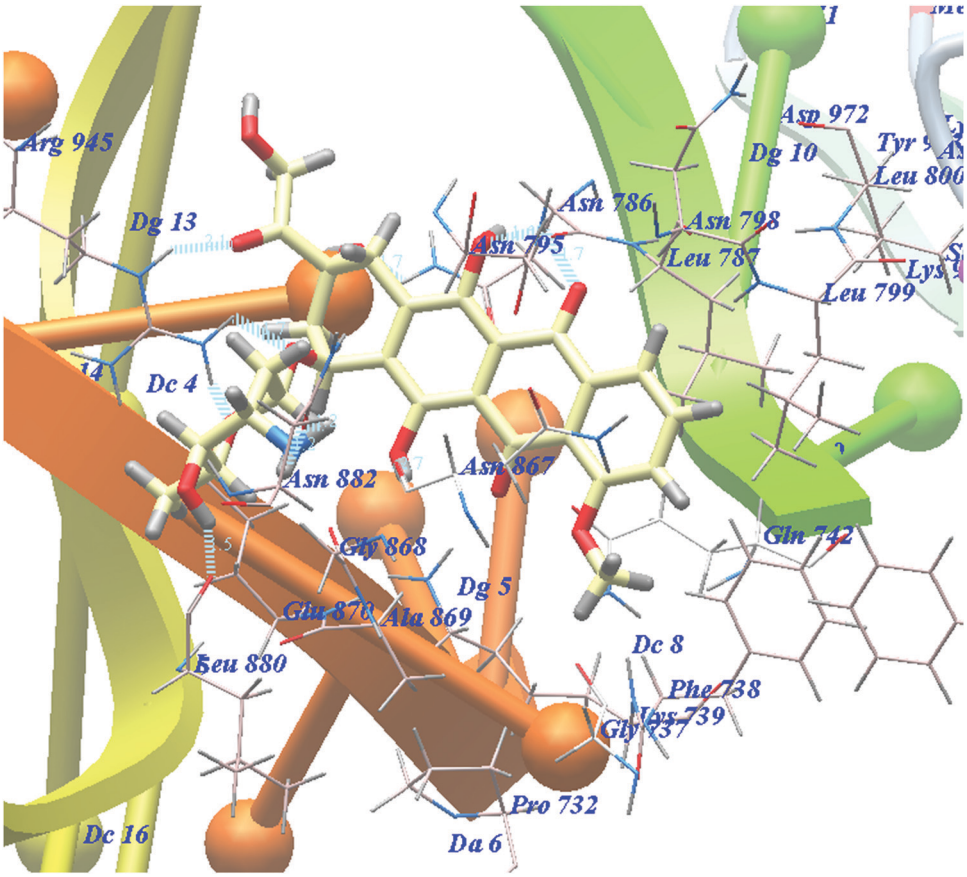

Fig. 3 Binding of doxorubicin with DNA; the hydrogen bonds are represented with blue dashed lines.

with Asparagine786) (Fig. 4). These interactions may explain the highest anticancer activity of $\mathbf{12_d}$.

The proposed binding mode of $\mathbf{12_a}$ exhibited an affinity value of −104.45 kcal mol^{-1} and nine H-bonds. The planar aromatic system occupied the hydrophobic pocket formed by Arginine945, Tyrosine908, Asparagine882, Glutamate870, Alanine869, Glycine868, Asparagine867, Lysine814, Asparagine798, Asparagine795, Glutamine789, Leucine787 and Asparagine786. It formed five H-bonds with the key amino acid Arginine945. It also stacked between the diphosphate cytidines (Dc3 and Dc4) and diphosphate guanosines (Dg5 and Dg13). The two substituted arms were oriented into the minor and major grooves of the DNA and were stabilized by the formation of four H-bonds with the key amino acids (one H-bond with Tyrosine908, one H-bond with Glutamine789 and two H-bonds with Lysine814) (Fig. 5). These interactions may explain the high anticancer activity of $\mathbf{12_a}$.

The proposed binding mode of $\mathbf{10_c}$ exhibited an affinity value of −89.88 kcal mol^{-1} and seven H-bonds. The planar aromatic system occupied the hydrophobic pocket formed by Arginine945, Tyrosine908, Asparagine882, Glutamate870, Alanine869, Glycine868, Asparagine867, Leucine799, Asparagine798, Asparagine795, Leucine787, Asparagine786, Glutamine742, Lysine739, Phenylalanine738, Glycine737 and Proline732. It formed two H-bonds with the key amino acids Asparagine786 and Asparagine795. It also stacked between the diphosphate cytidines (Dc3, Dc4, Dc1 and Dc19) and diphosphate guanosines (Dg2, Dg5 and Dg13). The 4-chlorophenyl moiety was oriented into the minor groove of the DNA. The side chain was stabilized by the formation of five H-bonds with the key amino acids (four H-bonds with Arginine945 and one H-bond with Glycine868) (Fig. 6).

As planned, the hydrophobic distal moieties and the long linkers and hydrogen bond acceptors present in the planar aromatic scaffold and/or the long chain linkers increased the affinity towards the DNA active site. From the obtained docking results (Table 1), we concluded that the $\mathbf{12_d}$ and $\mathbf{12_a}$ derivatives, which were designed as threading DNA intercalators due to having disubstituents at positions 1 and 5, exhibited the highest DNA intercalations. The benzylidene derivatives $\mathbf{10_c}$ and $\mathbf{10_d}$ showed increased hydrophobic interactions and, consequently, increased affinities towards the DNA active site, which may be due to the long chain linkers used. On the other hand, these modifications compensated for the hydrogen bonding and hydrophobic interactions of the reference drug doxorubicin.

2.3. *In vitro* anti-proliferative activity

The anti-proliferative activities of the seventeen newly synthesized [1,2,4]triazolo[4,3-*a*]quinoxaline derivatives $\mathbf{5–10_{a–e}}$ were examined against three human tumor cell lines, namely hepatocellular carcinoma (HepG2), colorectal carcinoma (HCT-116) and breast cancer (MCF-7), using the 3-[4,5-dimethylthiazol-2-yl]-2,5-diphenyltetrazolium bromide (MTT) colorimetric assay as

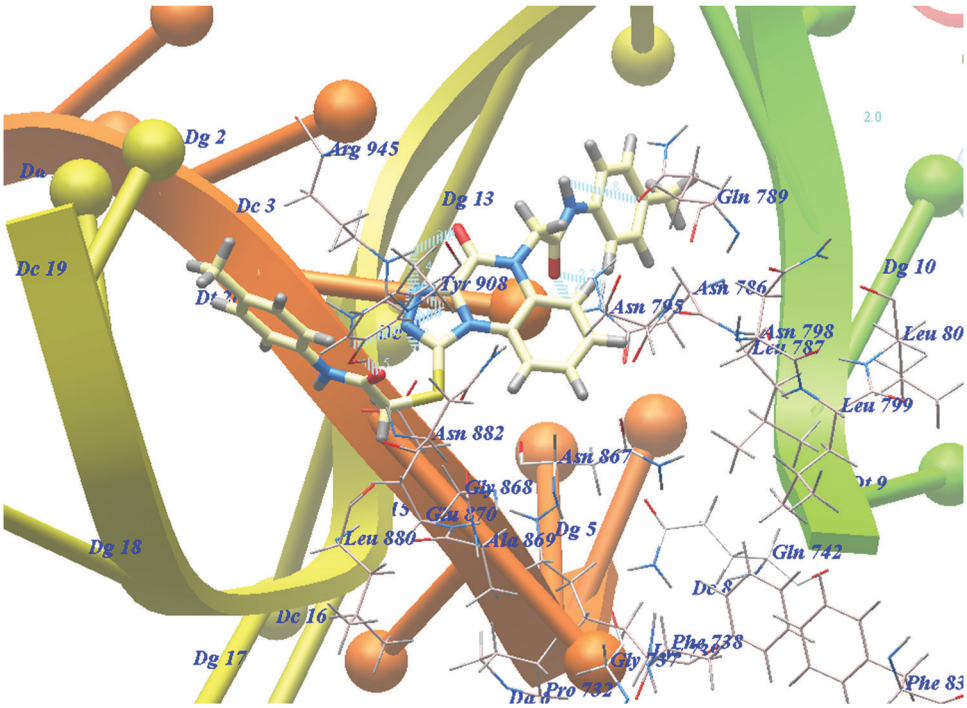

Fig. 4 Predicted binding mode of 12_d with DNA.

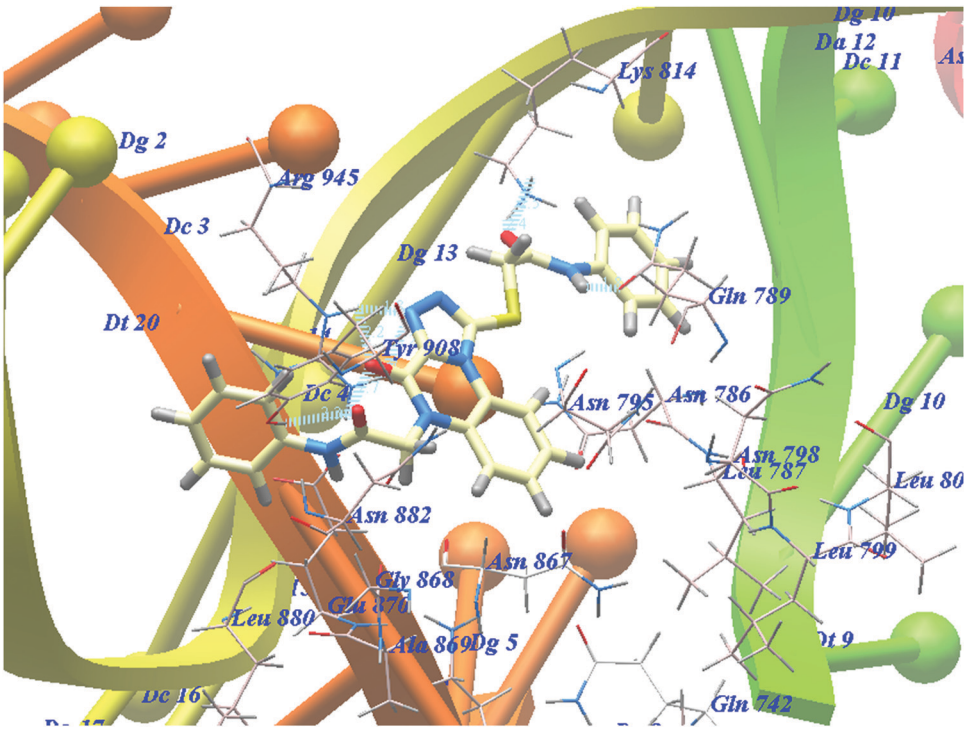

Fig. 5 Predicted binding mode of 12_a with DNA.

described by Mosmann.[33–35] Doxorubicin was included in the experiments as a reference cytotoxic drug. The results were expressed as the growth inhibitory concentration (IC_{50}) values and are summarized in Table 2. From the obtained results, it was explicated that most of the prepared compounds displayed very good to low growth inhibitory activity against the tested cancer cell lines. In general, the investigations of the cytotoxic activity indicated that MCF-7 was the most sensitive cell line to the

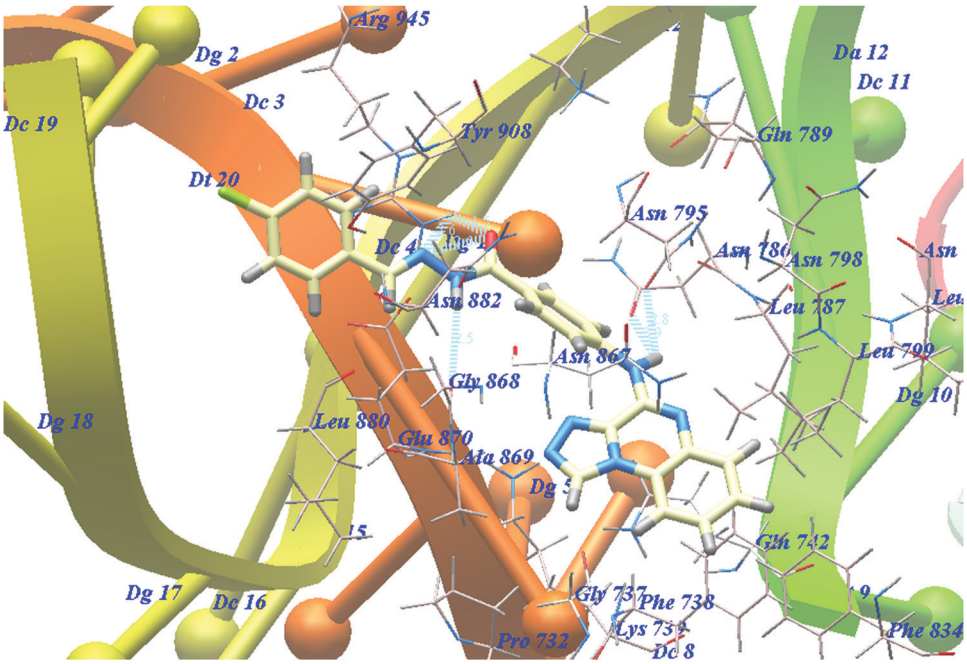

Fig. 6 Predicted binding mode of **10$_c$** with DNA.

Table 2 *In vitro* cytotoxic activities of the newly synthesized compounds against the HepG2, HCT-116, MCF-7 and VERO cell lines

	IC_{50}[a] (μM)			
Compound	HepG2	HCT116	MCF-7	VERO
7	40.69 ± 3.6	36.47 ± 3.3	32.91 ± 2.4	NT[b]
9	59.23 ± 3.9	47.30 ± 3.9	41.56 ± 3.0	NT[b]
10$_a$	69.56 ± 4.3	57.95 ± 4.2	49.16 ± 3.7	NT[b]
10$_b$	72.47 ± 4.4	61.87 ± 4.3	58.43 ± 4.2	NT[b]
10$_c$	33.41 ± 2.9	29.96 ± 2.5	24.78 ± 1.9	66.43 ± 0.22
10$_d$	37.55 ± 3.3	30.22 ± 2.6	25.53 ± 2.0	69.23 ± 0.22
10$_e$	85.19 ± 5.0	76.88 ± 4.9	64.79 ± 4.6	NT[b]
10$_f$	88.09 ± 5.1	66.62 ± 4.5	43.93 ± 3.1	NT[b]
10$_g$	89.79 ± 5.3	>100	76.38 ± 4.9	NT[b]
10$_h$	40.28 ± 3.6	35.12 ± 3.3	31.05 ± 2.5	70.54 ± 0.22
10$_i$	>100	>100	>100	NT[b]
10$_j$	79.37 ± 4.7	71.34 ± 4.8	59.61 ± 4.3	NT[b]
12$_a$	31.40 ± 2.8	28.81 ± 2.4	19.72 ± 1.5	65.12 ± 0.17
12$_b$	40.60 ± 4.2	36.33 ± 4.1	32.58 ± 3.6	73.12 ± 0.17
12$_c$	>100	>100	68.65 ± 5.2	NT[b]
12$_d$	22.08 ± 2.1	27.13 ± 2.2	17.12 ± 1.5	74.61 ± 0.19
12$_e$	>100	>100	93.89 ± 5.5	NT[b]
Doxorubicin	7.94 ± 0.6	8.07 ± 0.8	6.75 ± 0.4	NT[b]

[a] IC_{50} values are the mean ± S.D. of three separate experiments. [b] NT: Not tested.

influence of the new derivatives. In particular, compound **12$_d$** was found to be the most potent derivative of all the tested compounds against the three HepG2, HCT116 and MCF-7 cancer cell lines, with IC_{50} = 22.08 ± 2.1, 27.13 ± 2.2 and 17.12 ± 1.5 μM, respectively. Although this compound displayed nearly one third of the activity of doxorubicin (IC_{50} = 7.94 ± 0.6, 8.07 ± 0.8 and 6.75 ± 0.4 μM, respectively), it may be useful as a template for future design, optimization, and investigation to produce more potent anticancer analogs. On the other hand, compound **10$_i$** exhibited the lowest activity against the three HepG2, HCT116 and MCF-7 cancer cell lines, with the same IC_{50} values >100 μM.

With respect to the HepG2 hepatocellular carcinoma cell line, compounds **12$_a$**, **10$_c$** and **10$_d$** displayed very good anticancer activities, with IC_{50} values of 31.40 ± 2.8, 33.41 ± 2.9 and 37.55 ± 3.3 μM, respectively. Compounds **10$_h$**, **12$_b$** and **7**, with IC_{50} = 40.28 ± 3.6, 40.60 ± 4.2 and 40.69 ± 3.6 μM, respectively, displayed good cytotoxicity. Compounds **9**, **10$_a$** and **10$_b$**, with IC_{50} values ranging from 59.23 ± 3.9 to 72.47 ± 4.4 μM, exhibited moderate cytotoxicity. Meanwhile, compounds

10e, **10f**, **10g**, **10j**, **12c** and **12e**, with IC_{50} values ranging from 79.37 ± 4.7 to >100 μM, displayed the lowest cytotoxicity.

The cytotoxicity evaluation against the colorectal carcinoma (HCT-116) cell line revealed that compounds **12a**, **10c** and **10d** displayed very good anticancer activities, with IC_{50} values of 28.81 ± 2.4, 29.96 ± 2.5 and 30.22 ± 2.6 μM, respectively. Compounds **10h**, **12b**, **7** and **9**, with IC_{50} = 35.12 ± 3.3, 36.33 ± 4.1, 36.47 ± 3.3 and 47.30 ± 3.9 μM, respectively, displayed good cytotoxicity. Compounds **10a**, **10b**, **10f** and **10j**, with IC_{50} values ranging from 57.95 ± 4.2 to 71.34 ± 4.8 μM, exhibited moderate cytotoxicity. Meanwhile, compounds **10e**, **10g**, **12c** and **12e**, with IC_{50} values ranging from 76.88 ± 4.9 to >100 μM, displayed the lowest cytotoxicity.

The cytotoxicity evaluation against the MCF-7 cell line revealed that compounds **12a**, **10c** and **10d** displayed very good anticancer activities, with IC_{50} values of 19.72 ± 1.5, 24.78 ± 1.9 and 25.53 ± 2.0 μM, respectively. Compounds **10h**, **12b**, **7**, **9**, **10f** and **10a**, with IC_{50} = 31.05 ± 2.5, 32.58 ± 3.6, 32.91 ± 2.4, 41.56 ± 3.0, 43.93 ± 3.1 and 49.16 ± 3.7 μM, respectively, displayed good cytotoxicity. Compounds **10b**, **10e**, **10j** and **12c**, with IC_{50} values ranging from 58.43 ± 4.2 to 68.65 ± 5.2 μM, exhibited moderate cytotoxicity. Meanwhile, compounds **10g** and **12e**, with IC_{50} = 76.38 ± 4.9 and 93.89 ± 5.5 μM, respectively, displayed the lowest cytotoxicity.

Finally, the six most potent derivatives, **10c**, **10d**, **10h**, **12a**, **12b** and **12d**, were tested for their cytotoxicity against normal VERO cells. The results revealed that the tested compounds have low toxicity against normal VERO cells, with IC_{50} values ranging from 65.12 to 74.61 μM. The cytotoxicities of these compounds against the cancer cell lines ranged from 17.12 to 40.60 μM.

Compounds **10c**, **10d**, **10h**, **12a**, **12b** and **12d** are respectively 2.68, 2.71, 2.27, 3.30, 2.24 and 4.36 fold more toxic to breast cancer cells (MCF-7, the most sensitive cells) than to normal VERO cells.

2.4. *In vitro* DNA/methyl green assay

The most active anti-proliferative derivatives, **10c**, **10d**, **10h**, **12a**, **12b** and **12d**, were further evaluated for their DNA-binding affinities, which revealed the ability of these compounds to intercalate DNA. This investigation was carried out using methyl green dye according to the reported procedure described by Burre *et al.*[12,13,36] The results of the DNA-binding affinity were obtained as IC_{50} values and are summarized in Table 3. Doxorubicin, as one of the most powerful DNA intercalators, was used as a positive control.

The tested compounds displayed good to moderate DNA-binding affinities. Compound **12d** displayed the highest binding affinity. This compound potently intercalated DNA at a decreased IC_{50} value (35.33 ± 1.8 μM) which is nearly equipotent to that of doxorubicin (31.27 ± 1.8 μM). Compounds **12a** and **10c** exhibited good DNA-binding affinities, with IC_{50} values of 39.35 ± 3.9 and 42.35 ± 3.9 μM, respectively. Finally, compounds **10d**, **10h** and **12b** showed moderate DNA-binding affinities, with IC_{50} values of 50.35 ± 3.9, 57.08 ± 3.3 and 59.35 ± 3.2 μM, respectively.

Table 3 DNA intercalating affinities of the tested compounds

Compound	DNA binding IC_{50} (μM)	Compound	DNA binding IC_{50} (μM)
10c	42.35 ± 3.9	**12b**	59.35 ± 3.2
10d	50.35 ± 3.9	**12d**	35.33 ± 1.8
10h	57.08 ± 3.3	Doxorubicin	31.27 ± 1.8
12a	39.35 ± 3.9		

2.5. Structure–activity relationship (SAR)

The preliminary SAR study focused on the effects of the hydrophobic natures, electronic natures and positions of the substituents used in this study. Also, it focused on the effects of the number and length of linkers used and the presence of one and/or two distal moieties. The data obtained revealed that the tested compounds displayed different levels of anticancer activity and possessed a distinctive pattern of selectivity against the MCF-7 cell line. Generally, the [1,2,4]triazolo[4,3-*a*]quinoxaline scaffold, ester, acid hydrazide and/or acetamide linkers containing (HBA-HBD), lipophilicity and electronic nature exhibited important roles in DNA intercalation and, consequently, in the anticancer activity. The presence of two hydrophobic distal moieties linked to the chromophore through acetamide linkers, as in compounds **12a–e**, was found to be responsible for their higher anticancer activity than that of the other compounds containing only one hydrophobic distal moiety, as in compounds **7**, **8** and **10a–j**. The presence of two arms enables **12a–e** to form different hydrophobic and hydrophilic bonding interactions; one of the two arms is oriented into the minor groove of DNA and the other one is oriented into the major groove, as shown in molecular docking studies.

From the structure of the synthesized derivatives and the data shown in Table 2, we can divide these tested compounds into three groups. The first group is compounds **7** and **9**. In this group, short chain hydrophobic ester and hydrazide linkers were used. The ethyl ester derivative **7** showed higher activities than the acid hydrazide **9** against the three MCF-7, HCT116 and HepG2 cell lines, respectively. The second group is compounds **10a–j**; the terminal phenyl tail was unsubstituted, as in compound **10a**, or 2-substituted with a hydrophobic, electron-withdrawing chloro group and a hydrophobic, electron-donating methoxy group, as in compounds **10b** and **10g**, respectively. These compounds were also 4-substituted with different hydrophobic and/or hydrophilic electron-withdrawing groups, as in **10c** and **10d**, and/or electron-donating groups, as in **10h**. Compound **10e** was 2,6-disubstituted with two chloro groups. Moreover, compounds in this group were substituted with a hydrophobic, electron-withdrawing nitro group at positions 3 and/or 4, as in compounds **10i** and **10j**, respectively.

Within this group, the 4-substituted phenyl tail with a hydrophobic, electron-withdrawing chloro (+mesomeric effect (+M effect) and − inductive effect (−I effect)) group (**10c**) exhibited higher anticancer activities than the less hydrophobic, more electron-withdrawing fluoro (+M, −I) group (**10d**) and hydrophobic, electron-donating methoxy (+M, +I) group (**10h**) against the three MCF-7, HCT116 and HepG2 cell lines,

respectively. The unsubstituted derivative **10$_a$** exhibited higher activities than the 2-substituted derivative with the hydrophobic electron-withdrawing chloro (+M, −I) group (**10$_b$**) and that 4-substituted with a nitro (−M, −I) group (**10$_j$**) against the three MCF-7, HCT116 and HepG2 cell lines, respectively. The 2,6-dichloro-substituted compound **10$_e$** exhibited lower activities than the monosubstituted compounds against the three MCF-7, HCT116 and HepG2 cell lines, respectively. These findings obeyed the Hansch equation for the parabolic relationship between drug activity and hydrophobicity. The 4-substituted derivative with a hydrophilic electron-donating hydroxy (+M, −I) group (**10$_f$**) exhibited higher activities than that substituted at the 2-position with the hydrophobic, electron-donating methoxy (+M, +I) group (**10$_g$**) and that 3-substituted with the hydrophobic electron-withdrawing nitro (−M, −I) group (**10$_i$**), which indicates that the 4-position is critical to the activity.

In the third group, **12$_{a–e}$**, the 4-substituted terminal phenyl group with the hydrophobic electron-donating methyl (+I) group, as in **12$_d$**, exhibited higher activities than the unsubstituted **12$_a$** and the compound substituted with the hydrophobic electron-withdrawing chloro (+M, −I) group **12$_b$** and hydrophobic electron withdrawing nitro (−M, −I) group **12$_e$** against the three MCF-7, HCT116 and HepG2 cell lines, respectively. The 2,6-dichloro-substituted compound **12$_c$** showed lower activities than the monosubstituted compound **12$_b$** against the three MCF-7, HCT116 and HepG2 cell lines, respectively. These findings obeyed the Hansch equation for a parabolic relationship between drug activity and hydrophobicity and demonstrated that the 4-position is critical to the activity.

Based on the data obtained from DNA binding in Table 3, it can be concluded that the presence of two hydrophobic distal moieties linked to the chromophore through acetamide linkers,

Table 4 ADMET profiles of the four most active compounds and doxorubicin

Parameter	**10$_c$**	**10$_d$**	**12$_a$**	**12$_d$**	Doxorubicin
Molecular properties					
Molecular weight	441.882	425.427	484.541	512.595	543.525
log *P*	4.4384	3.9241	3.4137	4.03054	0.0013
Rotatable bonds	5	5	7	7	5
Acceptors	7	7	8	8	12
Donors	2	2	2	2	6
Surface area	187.133	180.995	203.350	216.080	222.081
Absorption					
Water solubility	−3.997	−3.684	−3.852	−3.897	−2.915
Caco2 permeability	1.097	1.25	0.622	0.424	0.457
Intestinal abs. (human)	92.827	92.132	90.728	91.679	62.372
Skin permeability	−2.735	−2.736	−2.736	−2.736	12.735
P-Glycoprotein substrate	Yes	Yes	Yes	Yes	Yes
P-Glycoprotein I inhibitor	Yes	Yes	Yes	Yes	No
P-Glycoprotein II inhibitor	Yes	Yes	Yes	Yes	No
Distribution					
VDss (human)	0.108	0.089	−0.181	−0.091	1.647
Fraction unbound (human)	0.062	0.097	0.156	0.191	0.215
BBB permeability	−0.565	−0.597	−0.715	−0.691	−1.379
CNS permeability	−1.947	−2.119	−2.416	−2.269	−4.307
Metabolism					
CYP2D6 substrate	No	No	No	No	No
CYP3A4 substrate	Yes	Yes	Yes	Yes	No
CYP1A2 inhibitor	Yes	Yes	Yes	No	No
CYP2C19 inhibitor	Yes	Yes	Yes	Yes	No
CYP2C9 inhibitor	Yes	Yes	Yes	Yes	No
CYP2D6 inhibitor	No	No	No	No	No
CYP3A4 inhibitor	Yes	Yes	Yes	Yes	No
Excretion					
Total clearance	−0.107	0.01	−0.028	−0.142	0.987
Renal OCT2 substrate	No	No	No	No	No
Toxicity					
AMES toxicity	Yes	Yes	No	No	No
Max. tolerated dose (human)	0.495	0.514	0.886	0.799	0.081
hERG I inhibitor	No	No	No	No	No
hERG II inhibitor	Yes	Yes	Yes	Yes	Yes
Oral rat acute toxicity (LD_{50})	2.64	2.628	2.581	2.585	2.408
Oral rat chronic toxicity (LOAEL)	1.308	1.287	1.82	1.59	3.339
Hepatotoxicity	Yes	Yes	Yes	Yes	Yes
Skin sensitization	No	No	No	No	No
T. pyriformis toxicity	0.286	0.285	0.287	0.287	0.285
Minnow toxicity	0.924	0.618	−1.87	−2.008	4.412

as in compounds **12d, a**, exhibited higher DNA binding activity than that of a single hydrophobic distal moiety, as in compounds **10c, d, h**. Compound **12d** 4-substituted with the hydrophobic electron-donating (+I) methyl group displayed higher activities than the unsubstituted compound **12a** and that substituted with a hydrophobic electron-withdrawing chloro (+M, −I) group (**12b**). Compound **10c** 4-substituted with the hydrophobic, electron-withdrawing chloro (+M, −I) group exhibited higher DNA binding activity than the less hydrophobic, more electron-withdrawing fluoro (+M, −I) group (**10d**) and the hydrophobic, electron-donating methoxy (+M, +I) group (**10h**).

2.6. *In silico* ADMET profiles

In the present study, a computational study of the four most active compounds (**12d, 12a, 10c** and **10d**) was conducted to determine their surface areas and other physicochemical properties[37] according to the directions of Lipinski's rule.[38] Lipinski suggested that the absorption of a compound is likely to be better if the molecule obeys at least three out of the following four rules: (i) HB donor groups ≤ 5; (ii) HB acceptor groups ≤ 10; (iii) molecular weight < 500; (iv) $\log P < 5$. In this study, whereas the reference anticancer agent doxorubicin violates three of Lipinski's rules, compound **12d** violates only one (molecular weight). All the most active derivatives have a number of hydrogen-bonding acceptor groups (7 and/or 8) and only 2 hydrogen-bonding donors, and these values agree with Lipinski's rules. Also, the absorption, distribution, metabolism, excretion, and toxicity (ADMET) profiles of the new synthesized derivatives were preliminarily assessed to analyze their potentials to serve as good medication candidates. The prediction of the ADMET profiles was conducted with the aid of the pkCSM descriptors algorithm protocol.[39]

After assessing the ADMET profiles of compounds **12d, 12a, 10c** and **10d** (Table 4), we can suggest that these derivatives have the advantage of better intestinal absorption in humans than doxorubicin (90.7–92.8, compared with 62.3 in the case of doxorubicin). This preference can be attributed to the superior lipophilicity of our designed ligands, which would facilitate their passage through different biological membranes.[40] Accordingly, these compounds may have significantly good bioavailability after oral administration. In the CNS permeability study, [1,2,4]triazolo[4,3-*a*]quinoxaline derivatives **12d, 12a, 10c** and **10d** demonstrated the best ability to penetrate the CNS (CNS permeability values −1.947 to −2.416), while doxorubicin is unable to penetrate the CNS (CNS permeability < -4.0). It is also clear that cytochrome P3A4, the main enzyme involved in drug metabolism, could be inhibited under the effects of compounds **12d, 12a, 10c** and **10d**, while doxorubicin could not. This may also be due to the higher lipophilicity of our new ligands. Excretion was assessed in term of the total clearance, which is a significant parameter in deciding dose intervals. The obtained data revealed that doxorubicin revealed the highest total clearance value compared to the other ligands. On the other hand, the new ligands showed lower total clearance values. Thus, doxorubicin can be excreted more quickly and accordingly requires shorter dosing intervals. Dissimilar to doxorubicin, the new compounds exhibited slower clearance rates, which indicates the possibility of preferential extended dosing intervals of the novel derivatives. The last parameter examined in the ADMET profiles of our newly synthesized VEGFR-2 inhibitors is toxicity. As displayed in Table 4, doxorubicin and all the new ligands shared the drawback of unwanted hepatotoxic effects. In terms of the maximum tolerated dose in humans, the new [1,2,4]triazolo[4,3-*a*]quinoxaline derivatives **12d, 12a, 10c** and **10d** showed values 9.86, 10.94, 6.11 and 6.35 fold that of the reference compound doxorubicin, respectively, which indicates the advantage of the wide therapeutic index of the new derivatives. Finally, the oral acute toxic doses of the new compounds (LD_{50}) are slightly greater than that of the reference drug (2.581–2.64 for our new derivatives compared with 2.40 for doxorubicin).

3. Conclusion

In summary, seventeen new [1,2,4]triazolo[4,3-*a*]quinoxaline based derivatives have been designed, synthesized and evaluated for their anticancer activities against three human tumor cell lines, namely hepatocellular carcinoma (HepG2), colorectal carcinoma (HCT-116) and breast cancer (MCF-7), as DNA intercalators. The tested compounds showed variable anticancer activities. Molecular docking studies were performed to investigate the binding modes of the proposed compounds with the DNA active site. The data obtained from the biological testing highly correlated with those obtained from the molecular modeling studies.

In general, the investigations of the cytotoxic activity indicated that MCF-7 was the most sensitive cell line to the influence of the new derivatives. In particular, compound **12d** was found to be the most potent derivative of all the tested compounds against the three HepG2, HCT116 and MCF-7 cancer cell lines, with IC_{50} = 22.08 ± 2.1, 27.13 ± 2.2 and 17.12 ± 1.5 μM, respectively. Although this compound displayed nearly one third of the activity of doxorubicin (IC_{50} = 7.94 ± 0.6, 8.07 ± 0.8 and 6.75 ± 0.4 μM, respectively), it may be useful as a template for future design, optimization, and investigation to produce more potent anticancer analogs. Compounds **12a, 10c** and **10d** displayed very good anticancer activities against the three HepG2, HCT116 and MCF-7 cancer cell lines, with IC_{50} = 31.40 ± 2.8, 28.81 ± 2.4 and 19.72 ± 1.5 μM for **12a**, 33.41 ± 2.9, 29.96 ± 2.5 and 24.78 ± 1.9 μM for **10c**, and 37.55 ± 3.3, 30.22 ± 2.6 and 25.53 ± 2.0 μM for **10b**, respectively.

The most active derivatives, **10c, 10d, 10h, 12a, 12b** and **12d**, were evaluated for their DNA binding activities. Compound **12d** displayed the highest binding affinity. This compound potently intercalates DNA at a decreased IC_{50} value (35.33 ± 1.8 μM) which is nearly equipotent to that of doxorubicin (31.27 ± 1.8 μM). Compounds **12a** and **10c** exhibited good DNA-binding affinities, with IC_{50} values of 39.35 ± 3.9 and 42.35 ± 3.9 μM, respectively. Finally, compounds **10d, 10h** and **12b** showed moderate DNA-binding affinities, with IC_{50} values of 50.35 ± 3.9, 57.08 ± 3.3 and 59.35 ± 3.2 μM respectively.

Also, compounds **10c**, **10d**, **10h**, **12a**, **12b** and **12d** are respectively 2.68, 2.71, 2.27, 3.30, 2.24 and 4.36 fold more toxic in breast cancer cells (MCF-7, the most sensitive cells) than in normal VERO cells.

Furthermore, ADMET profiles were calculated for the four most active compounds in comparison to doxorubicin as a reference drug.

4. Experimental

4.1. Chemistry

4.1.1. General. All melting points were determined by the open capillary method on a Gallenkamp melting point apparatus at the Faculty of Pharmacy of Al-Azhar University and were uncorrected. The infrared spectra were recorded on a Pye Unicam SP 1000 IR spectrophotometer at the Pharmaceutical Analytical Unit, Faculty of Pharmacy, Al-Azhar University, using the potassium bromide disc technique. Proton magnetic resonance ^{1}H NMR spectra were recorded on a Bruker 400 Megahertz-nuclear magnetic resonance (400 MHz-NMR) spectrophotometer at the Microanalytical Unit, Faculty of Pharmacy, Ain Shams University, and on a GEMINI-400BB NMR spectrometer at the Chemical Laboratories of the Ministry of Defense, Cairo. Carbon-13 (C13) nuclear magnetic resonance (^{13}C NMR) spectra were recorded on a Bruker 100 megahertz-nuclear magnetic resonance (100 MHz-NMR) spectrophotometer at the Microanalytical Unit, Faculty of Pharmacy, Cairo University. Tetramethylsilane (TMS) was used as the internal standard, and the chemical shifts were measured on a δ scale in parts per million (ppm). The mass spectra were carried out on the Direct Probe Controller Inlet part of a single quadrupole mass analyzer (Thermo Scientific Gas chromatography-mass spectrometry (GCMS) model ISQ LT) using Thermo X-Calibur software at the Mycology and Biotechnology Regional Center, Al-Azhar University. Elemental analyses (C, H, N) were performed on a carbon hydrogen and nitrogen (CHN) analyzer at the Mycology and Biotechnology Regional Center, Al-Azhar University. All compounds were within $\pm$0.4 of the theoretical values. The reactions were monitored by thin-layer chromatography (TLC) using TLC sheets precoated with Merck 60 F254 UV fluorescent silica gel plates and were visualized using an ultraviolet (UV) lamp and different solvents as mobile phases.

Compounds 2,3-(1*H*,4*H*)-quinoxalinedione **3**, 2,3-dichloroquinoxaline **4**, 2-chloro-3-hydrazinylquinoxaline **5**, 4-chloro[1,2,4]triazolo[4,3-*a*]quinoxaline **6**, 4-chloro-[1,2,4]triazolo[4,3-*a*]quinoxaline-1-thiol **8** and potassium 4-oxo-1-sulfido-4*H*-[1,2,4]triazolo[4,3-*a*]quinoxalin-5-ide **11** were obtained according to the reported procedures.[13,30]

4.1.2. Methyl 4-([1,2,4]triazolo[4,3-*a*]quinoxalin-4-ylamino) benzoate (7). Equimolar quantities of 4-chloro-[1,2,4]triazolo[4,3-*a*]quinoxaline **6** (2.04 g, 0.01 mol) and methyl 4-aminobenzoate (1.51 g, 0.01 mol) in acetonitrile (CH_3CN) (20 ml) in the presence of a few drops of triethylamine (TEA) were heated under reflux for 5 h. The formed precipitate was filtered, washed with *n*-hexane, and air dried to obtain the corresponding methyl ester derivative **7**.

Yield, 90%; m.p. 170–2 °C; IR$_{\nu_{max}}$ (cm^{-1}): 3243 (NH), 3090 (C–H aromatic), 2965 (C–H aliphatic), 1725 (CO ester); ^{1}H NMR (400 MHz, DMSO-d$_6$): 3.83 (s, 3H, CH_3), 7.40–7.44 (dd, H, H-7 quinox.), 7.46–7.49 (dd, 1H, H-8 quinox.), 7.70–7.72 (d, 1H, H-9 quinox.), 7.88–7.90 (dd, 2H, H-3 and H-5 phenyl), 8.17–819 (d, 1H, H-6 quinox.), 8.31–8.33 (dd, 2H, H-2 and H-6 phenyl), 10.01 (s, 1H, CH triazole), 10.53 (s, 1H, **NH**-ph) (D_2O exchangeable); anal. calcd for $C_{17}H_{13}N_5O_2$ (319.32): C, 63.94; H, 4.10; N, 21.93. Found: C, 64.08; H, 4.23; N, 21.88.

4.1.3. 4-([1,2,4]Triazolo[4,3-*a*]quinoxalin-4-ylamino)benzohydrazide (9). A mixture of the ester derivative **7** (9.6 g, 0.03 mol) and hydrazine hydrate 80% (6.0 g, 0.12 mol) in ethanol (150 ml) was stirred well and refluxed for 8 h. The solvent was evaporated and the obtained solid was filtered, washed with water several times, dried and re-crystallized from ethanol to afford the corresponding hydrazide derivative (**9**).

Yield, 80%; m.p. 293–5 °C; IR$_{\nu_{max}}$ (cm^{-1}): 3299, 3229 (2NH, NH2), 3054 (C–H aromatic), and 1660 (CO amide); ^{1}H NMR (400 MHz, DMSO-d$_6$): 4.48 (s, 2H, NH_2) (D_2O exchangeable), 7.44–7.48 (dd, 1H, H-7 quinox.), 7.51–7.55 (dd, 1H, H-8 quinox.), 7.76–7.78 (d, 1H, H-9 quinox.), 7.86–7.88 (dd, 2H, H-3 and H-5 phenyl), 8.22–8.24 (d, 1H, H-6 quinox.), 8.28–8.30 (dd, 2H, H-2 and H-6 phenyl), 9.71 (s, 2H, CH triazole and **NH**-ph (D_2O exchangeable)), 10.05 (s, 1H, **NH**-NH_2) (D_2O exchangeable); MS (*m*/*z*): 319 (M^+, $C_{16}H_{13}N_7O$, 18.98%), 288 (base peak, 100%), 231 (37.76%), 89 (10.02%), and 74 (31.33%); anal. calcd for $C_{16}H_{13}N_7O$ (319.33): C, 60.18; H, 4.10; N, 30.70. Found: C, 60.34; H, 4.37; N, 30.97.

4.1.4. General procedure for the synthesis of target compounds 10a–j. Equimolar amounts of acid hydrazide derivative **9** (0.5 g, 0.0015 mol) and the appropriate benzaldehyde derivatives, namely benzaldehyde, 2-chlorobenzaldehyde, 4-chlorobenzaldehyde, 4-fluorobenzaldehyde, 2,6-dichlorobenzaldehyde, 4-hydroxybenzaldehyde, 2-methoxybenzaldehyde, 4-methoxybenzaldehyde, 3-nitrobenzaldehyde, and/or 4-nitrobenzaldehyde (0.0015 mol), were refluxed in ethanol (25 ml) in the presence of few drops of glacial acetic acid for 4 h. The mixture was cooled, and the formed solid was filtered and re-crystallized from ethanol to furnish the corresponding Schiff bases **10a–j**, respectively.

*4.1.4.1. 4-([1,2,4]Triazolo[4,3-a]quinoxalin-4-ylamino)-N′-benzylidenebenzohydrazide (**10a**).* Yield, 90%; m.p. 254–6 °C; IR$_{\nu_{max}}$ (cm^{-1}): 3254, 3115 (2NH), 3060 (C–H aromatic), and 1631 (CO); ^{1}H NMR (400 MHz, DMSO-d$_6$): 7.44–7.49 (m, 3H, H-3, H-4 and H-5 of C_6H_5), 7.52–7.56 (dd, 1H, H-7 quinox.), 7.73–7.75 (dd, 1H, H-8 quinox.), 7.77–7.79 (d, 1H, H-9 quinox.), 7.98–8.00 (dd, 2H, H-3 and H-5 C_6H_4), 8.24–8.26 (dd, 2H, H-2 and H-6 C_6H_4), 8.37 (d, 1H, H-6 quinox.), 8.39 (dd, 2H, H-2 and H-6 of C_6H_5), 8.49 (s, 1H, NHN=**CH**-ph), 10.08 (s, 1H, CH triazolo), 10.57 (s, 1H, **NH**-ph) (D_2O exchangeable), 11.82 (s, 1H, NH of CO**NH**–N=) (D_2O exchangeable); anal. calcd for $C_{23}H_{17}N_7O$ (407.44): C, 67.80; H, 4.21; N, 24.06. Found: C, 68.12; H, 4.36; N, 24.13.

*4.1.4.2. 4-([1,2,4]Triazolo[4,3-a]quinoxalin-4-ylamino)-N′-(2-chlorobenzylidene)benzohydrazide (**10b**).* Yield, 95%; m.p. 285–

7 °C; $IR_{\nu_{max}}$ (cm^{-1}): 3333, 3177 (2NH), 3060 (C–H aromatic), and 1646 (CO); ^1H NMR (400 MHz, DMSO-d_6): 7.42–7.44 (dd, 1H, H-5′), 7.45–7.48 (m, 2H, H-3′ and H-4′), 7.49–7.51 (dd, 1H, H-7 quinox.), 7.52–7.54 (dd, 1H, H-8 quinox.), 7.56–7.58 (d, 1H, H-9 quinox.), 7.78–7.81 (dd, 2H, H-3 and H-5 phenyl), 7.96–8.02 (dd, 2H, H-2 and H-6 phenyl), 8.26–8.28 (d, 1H, H-6 quinox.), 8.36–8.38 (d, 1H, H-6′), 8.87 (s, 1H, NHN=**CH**-ph), 10.07 (s, 1H, CH triazolo), 10.57 (s, 1H, **NH**-ph) (D_2O exchangeable), 12.00 (s, 1H, NH of CO**NH**–N=) (D_2O exchangeable); anal. calcd for $C_{23}H_{16}ClN_7O$ (441.88): C, 62.52; H, 3.65; N, 22.19. Found: C, 62.69; H, 3.81; N, 22.37.

*4.1.4.3. 4-([1,2,4]Triazolo[4,3-a]quinoxalin-4-ylamino)-N′-(4-chlorobenzylidene)benzohydrazide (**10$_c$**).* Yield, 95%; m.p. 280–2 °C; $IR_{\nu_{max}}$ (cm^{-1}): 3242, 3177 (2NH), 3090 (C–H aromatic), and 1650 (CO); ^1H NMR (400 MHz, DMSO-d_6): 7.48–7.50 (dd, 2H, H-3′ and H-5′), 7.51–7.53 (dd, 1H, H-7 quinox.), 7.55–7.57 (dd, 1H, H-8 quinox.), 7.75–7.77 (d, 1H, H-9 quinox.), 7.79–7.81 (dd, 2H, H-3 and H-5 phenyl), 7.97–7.99 (dd, 2H, H-2 and H-6 phenyl), 8.26–8.28 (d, 1H, H-6 quinox.), 8.37–8.39 (dd, 2H, H-2′ and H-6′), 8.46 (s, 1H, NHN=**CH**-ph), 10.08 (s, 1H, CH triazolo), 10.58 (s, 1H, **NH**-ph) (D_2O exchangeable), 11.86 (s, 1H, NH of CO**NH**–N=) (D_2O exchangeable); MS (*m*/*z*): 443 (M^{2+}, 1.65%), 441 (M^+, 4.94%), 231 (48%), 318 (base peak, 100%), and 287 (60.69%); anal. calcd for $C_{23}H_{16}ClN_7O$ (441.88): C, 62.52; H, 3.65; N, 22.19. Found: C, 62.73; H, 3.79; N, 22.42.

*4.1.4.4. 4-([1,2,4]Triazolo[4,3-a]quinoxalin-4-ylamino)-N′-(4-fluorobenzylidene)benzohydrazide (**10$_d$**).* Yield, 85%; m.p. 273–5 °C; $IR_{\nu_{max}}$ (cm^{-1}): 3331, 3194 (2NH), 3070 (C–H aromatic), and 1644 (CO); ^1H NMR (400 MHz, DMSO-d_6): 7.29–7.31 (dd, 1H, H-3′ and H-5′), 7.45–7.47 (dd, 1H, H-7 quinox.), 7.50–7.52 (dd, 1H, H-8 quinox.), 7.55–7.57 (d, 1H, H-9 quinox.), 7.77–7.79 (dd, 2H, H-3 and H-5 phenyl), 7.97–7.99 (dd, 2H, H-2 and H-6 phenyl), 8.24–8.26 (d, 1H, H-6 of quinox.), 8.37–8.39 (dd, 2H, H-2′ and H-6′), 8.48 (s, 1H, NHN=**CH**-ph), 10.08 (s, 1H, CH triazolo), 10.55 (s, 1H, **NH**-ph) (D_2O exchangeable), 11.81 (s, 1H, NH of CO**NH**–N=) (D_2O exchangeable); anal. calcd for $C_{23}H_{16}FN_7O$ (425.43): C, 64.94; H, 3.79; N, 23.05. Found: C, 65.21; H, 3.86; N, 23.18.

*4.1.4.5. 4-([1,2,4]Triazolo[4,3-a]quinoxalin-4-ylamino)-N′-(2,6-dichlorobenzylidene)benzohydrazide (**10$_e$**).* Yield, 90%; m.p. 292–4 °C; $IR_{\nu_{max}}$ (cm^{-1}): 3188 (2NH), 3060 (C–H aromatic), and 1686 (CO); ^1H NMR (400 MHz, DMSO-d_6): 7.41–7.45 (t, 1H, H-4′), 7.47–7.49 (dd, 1H, H-7 quinox.), 7.49–7.51 (dd, 1H, H-8 quinox.), 7.54–7.56 (d, 1H, H-9 quinox.), 7.79–7.81 (dd, 2H, H-3 and H-5 phenyl), 7.96–7.98 (dd, 2H, H-2 and H-6 phenyl), 8.25–8.27 (d, 1H, H-6 of quinox.), 8.36–8.38 (dd, 2H, H-3′ and H-5′), 8.66 (s, 1H, NHN=**CH**-ph), 10.07 (s, 1H, CH triazolo), 10.57 (s, 1H, **NH**-ph) (D_2O exchangeable), 12.05 (s, 1H, NH CO**NH**–N=) (D_2O exchangeable); anal. calcd for $C_{23}H_{15}Cl_2N_7O$ (476.39): C, 58.00; H, 3.17; N, 20.58. Found: 57.89; H, 3.40; N, 20.79.

*4.1.4.6. 4-([1,2,4]Triazolo[4,3-a]quinoxalin-4-ylamino)-N′-(4-hydroxybenzylidene)benzohydrazide (**10$_f$**).* Yield, 80%; m.p. 294–6 °C; $IR_{\nu_{max}}$ (cm^{-1}): 3336, 3221 (2NH), 3085 (C–H aromatic), and 1658 (CO); ^1H NMR (400 MHz, DMSO-d_6): 6.82–6.84 (dd, 2H, H-3′ and H-5′), 7.47–7.49 (dd, 1H, H-7 of quinox.), 7.51–7.53 (dd, 1H, H-8 quinox.), 7.56–7.58 (d, H, H-9 quinox.), 7.79–7.80 (dd, 2H, H-3 and H-5 phenyl), 7.92–7.94 (dd, 2H, H-2 and H-6 phenyl), 8.25–8.27 (d, 1H, H-6 quinox.), 8.33–8.35 (dd, 2H, H-2′ and H-6′), 8.36 (s, 1H, NHN=**CH**-ph), 9.89 (s, 1H, **OH**) (D_2O exchangeable), 10.06 (s, 1H, CH triazolo), 10.54 (s, 1H, **NH**-ph) (D_2O exchangeable), 11.55 (s, 1H, NH of CO**NH**–N=) (D_2O exchangeable); anal. calcd for $C_{23}H_{17}N_7O_2$ (423.14): C, 65.24; H, 4.05; N, 23.16. Found: C, 65.38; H, 4.23; N, 23.50.

*4.1.4.7. 4-([1,2,4]Triazolo[4,3-a]quinoxalin-4-ylamino)-N′-(2-methoxybenzylidene)benzohydrazide (**10$_g$**).* Yield, 90%; m.p. 257–9 °C; $IR_{\nu_{max}}$ (cm^{-1}): 3259, 3107 (2NH), 3094 (C–H aromatic), 2950 (C–H aliphatic), and 1676 (CO); ^1H NMR (400 MHz, DMSO-d_6): 3.86 (s, 3H, CH_3), 7.02 (d, 1H, H-3′), 7.09–7.11 (dd, 1H, H-5′), 7.40 (dd, 1H, H-7 quinox.), 7.49–7.51 (dd, 1H, H-8 quinox.), 7.54–7.56 (d, 1H, H-9 quinox.), 7.79–7.81 (dd, 2H, H-3 and H-5 phenyl), 7.95–7.97 (dd, 2H, H-2 and H-6 phenyl), 8.26–8.28 (d, 1H, H-6 quinox.), 8.34–8.36 (dd, 2H, H-4′ and H-6′), 8.81 (s, 1H, NHN=**CH**-ph), 10.07 (s, 1H, CH triazolo), 10.55 (s, 1H, **NH**-ph) (D_2O exchangeable), 11.76 (s, 1H, NH of CO**NH**–N=) (D_2O exchangeable); MS (*m*/*z*): 437 (M^+, $C_{24}H_{19}N_7O_2$, 11.32%), 318 (98.09%), 288 (base peak, 100%), 104 (66.46%) and 89 (17.16%); anal. calcd for $C_{24}H_{19}N_7O_2$ (437.46): C, 65.89; H, 4.38; N, 22.41. Found: C, 66.11; H, 4.57; N, 22.32.

*4.1.4.8. 4-([1,2,4]Triazolo[4,3-a]quinoxalin-4-ylamino)-N′-(4-methoxybenzylidene)benzohydrazide (**10$_h$**).* Yield, 95%; m.p. 280–2 °C; $IR_{\nu_{max}}$ (cm^{-1}): 3258, 3134 (2NH), 3090 (C–H aromatic), 2969 (CH-aliphatic), and 1676 (CO); ^1H NMR (400 MHz, DMSO-d_6): 3.84 (s, 3H, CH_3), 7.02–7.04 (dd, 2H, H-3′ and H-5′), 7.49–7.52 (dd, 1H, H-7 quinox.), 7.55–7.59 (dd, 1H, H-8 quinox.), 7.67–7.70 (d, 1H, H-9 quinox.), 7.80–7.82 (dd, 2H, H-3 and H-5 phenyl), 7.95–7.98 (dd, 2H, H-2 and H-6 phenyl), 8.26–8.28 (d, 1H, H-6 quinox.), 8.36–8.39 (dd, 2H, H-2′ and H-6′), 8.42 (s, 1H, NHN=**CH**-ph), 10.10 (s, 1H, CH triazolo), 10.58 (s, 1H, **NH**-ph) (D_2O exchangeable), 11.66 (s, 1H, NH CO**NH**–N=) (D_2O exchangeable); ^{13}C NMR (100 MHz, DMSO-d_6): 55.76, 114.80 (2), 116.72, 120.72 (2), 123.17 (2), 125.64, 127.49, 127.54, 128.18, 128.72 (2), 129.08 (2), 136.25, 138.78, 138.83, 148.24, 143.40, 147.68, 161.22, 162.97; anal. calcd for $C_{24}H_{19}N_7O_2$ (437.46): C, 65.89; H, 4.38; N, 22.41. Found: C, 65.97; H, 4.62; N, 22.48.

*4.1.4.9. 4-([1,2,4]Triazolo[4,3-a]quinoxalin-4-ylamino)-N′-(3-nitrobenzylidene)benzohydrazide (**10$_i$**).* Yield, 80%; m.p. 295–7 °C; $IR_{\nu_{max}}$ (cm^{-1}): 3395, 3268 (2NH), 3090 (C–H aromatic), and 1681 (CO); ^1H NMR (400 MHz, DMSO-d_6): 7.50–7.52 (dd, 1H, H-5′), 7.56–7.58 (d, 1H, H-4′), 7.74–7.76 (dd, 1H, H-7 quinox.), 7.79–7.81 (dd, 1H, H-8 quinox.), 7.96–7.98 (d, 1H, H-9 quinox.), 8.14–8.16 (dd, 1H, H-6′), 8.23–8.25 (dd, 2H, H-3 and H-5 phenyl), 8.26–8.28 (dd, 2H, H-2 and H-6 phenyl), 8.37–8.39 (d, 1H, H-6 quinox.), 8.54 (s, 1H, H-2′), 8.57 (s, 1H, NHN=**CH**-ph), 10.07 (s, 1H, CH triazolo), 10.58 (s, 1H, **NH**-ph) (D_2O exchangeable), 12.03 (s, 1H, NH of CO**NH**–N=) (D_2O exchangeable); anal. calcd for $C_{23}H_{16}N_8O_3$ (452.43): C, 61.06; H, 3.56; N, 24.77. Found: C, 61.30; H, 3.69; N, 24.96.

*4.1.4.10. 4-([1,2,4]Triazolo[4,3-a]quinoxalin-4-ylamino)-N′-(4-nitrobenzylidene)benzohydrazide (**10$_j$**).* Yield, 85%; m.p. 300–2 °C; IR$_{\nu_{max}}$ (cm^{-1}): 3300, 3197 (2NH), 3060 (C–H aromatic), 1686 and (CO); ^{1}H NMR (400 MHz, DMSO-d$_6$): 52–7.54 (dd, 2H, H-3′ and H-5′), 7.55–7.58 (dd, 1H, H-7quinox.), 7.59–7.61 (dd, 1H, H-8 quinox.), 7.81–7.83 (d, 1H, H-9 quinox.), 7.85–7.87 (dd, 2H, H-3 and H-5 phenyl), 8.28–8.30 (dd, 2H, H-2 and H-6 phenyl), 8.31–8.33 (d, 1H, H-6 quinox.), 8.39–8.42 (dd, 2H, H-2′ and H-6′), 8.59 (s, 1H, NHN=**CH**-ph), 10.09 (s, 1H, CH triazolo), 10.61 (s, 1H, **NH**-ph) (D$_2$O exchangeable), 12.11 (s, 1H, NH of CO**NH**–N=) (D$_2$O exchangeable); anal. calcd for $C_{23}H_{16}N_8O_3$ (452.43): C, 61.06; H, 3.56; N, 24.77. Found: C, 61.25; H, 3.74; N, 24.59.

4.1.5. General procedure for synthesis of target compounds (12$_{a–e}$). The appropriate 2-chloroacetanilides, namely 2-chloroacetanilide, 2-chloro-4-chloroacetanilide, 2-chloro-2,6-dichloroacetanilide, 2-chloro-4-methylacetanilide, and 2-chloro-4-nitroacetanilide, (0.002 mol), were added to the dipotassium salt (**11**) (0.5 g, 0.001 mol) in DMF (10 ml), and the reaction mixture was heated under reflux for 3 h. The reaction mixture was poured on crushed ice, and the resulting precipitate was filtered and crystallized from ethanol to obtain the corresponding di-substituted derivatives **12$_{a–e}$**, respectively.

*4.1.5.1. 2-(4-Oxo-1-{(2-oxo-2-[phenylamino]ethyl)thio}-[1,2,4]triazolo[4,3-a]quinoxalin-5(4H)-yl)-N-phenylacetamide (**12$_a$**).* Yield, 90%; m.p. 183–5 °C; IR$_{\nu_{max}}$ (cm^{-1}): 3264 (2NH), 3057 (C–H aromatic), 2927 (C–H aliphatic), 1667 (3 CO); ^{1}H NMR (400 MHz, DMSO-d$_6$): 4.39 (s, 2H, S-CH$_2$), 4.49 (s, 2H, N-CH$_2$), 7.60–8.57 (m, 14H, aromatic protons), 10.72 (s, 1H, NH) (D$_2$O exchangeable), 10.81 (s, 1H, NH) (D$_2$O exchangeable); ^{13}C NMR (100 MHz, DMSO-d$_6$): 20.91, 34.36, 116.66, 119.65 (2), 119.66 (2), 125.35 (2C), 128.26, 128.49, 129.63, 132.86 (2), 133.01 (2), 136.23, 136.95 (2), 144.04, 146.99, 152.05 (2) 165.30, 165.94; MS (*m*/*z*): 484 (M$^+$, 8.50%), 337 (44.91%), 236 (45.20%), 102 (45.89%), 91 (base peak, 100%), and 78 (83.16%); anal. calcd for $C_{25}H_{20}N_6O_3S$ (484.53): C, 61.97; H, 4.16; N, 17.34. Found: C, 62.31; H, 4.28; N, 17.60.

*4.1.5.2. N-(4-Chlorophenyl)-2-{(5-[2-{(4-chlorophenyl)amino}-2-oxoethyl]-4-oxo-4,5-dihydro-[1,2,4]triazolo-[4,3-a]quinoxalin-1-yl)thio}acetamide (**12$_b$**).* Yield, 90%; m.p. 265–7 °C; IR$_{\nu_{max}}$ (cm^{-1}): 3298 (2NH), 3090 (C–H aromatic), 2947 (C–H aliphatic), 1689 (3 CO); ^{1}H NMR (400 MHz, DMSO-d$_6$): 4.39 (s, 2H, S-CH$_2$), 4.56 (s, 2H, N-CH$_2$) 7.59–8.58 (m, 12H, aromatic protons), 10.71 (s, 1H, NH) (D$_2$O exchangeable), 10.79 (s, 1H, NH) (D$_2$O exchangeable); anal. calcd for $C_{25}H_{18}Cl_2N_6O_3S$ (553.42): C, 54.26; H, 3.28; N, 15.19. Found: C, 54.89; H, 3.48; N, 15.02.

*4.1.5.3. N-(2,6-Dichlorophenyl)-2-{(5-[2-{(2,6-dichlorophenyl)amino}-2-oxoethyl]-4-oxo-4,5-dihydro-[1,2,4]triazolo[4,3-a]quinoxalin-1-yl)thio}acetamide (**12$_c$**).* Yield, 95%; m.p. 217–9 °C; IR$_{\nu_{max}}$ (cm^{-1}): 3289 (2NH), 3009 (C–H aromatic), 2925 (C–H aliphatic), 1683 (3 CO); ^{1}H NMR (400 MHz, DMSO-d$_6$): 4.51 (s, 4H, 2CH$_2$), 7.52–8.71 (m, 10H, aromatic protons), 10.35 (s, 1H, NH) (D$_2$O exchangeable), 11.03 (s, 1H, NH) (D$_2$O exchangeable); MS (*m*/*z*): 622 (M$^+$, 6.43%), 608 (17.98%), 520 (23.19%), 368 (67.37%), 77 (61.19%), 70 (base peak, 100%), and 78 (83.16%); anal. calcd for $C_{25}H_{16}Cl_4N_6O_3S$ (622.302): C, 48.25; H, 2.59; N, 13.51. Found: C, 48.03; H, 2.87; N, 13.74.

*4.1.5.4. 2-{4-Oxo-1-([2-oxo-2-{p-tolylamino}ethyl]thio)-[1,2,4]triazolo[4,3-a]quinoxalin-5(4H)-yl}-N-(p-tolyl)acetamide (**12$_d$**).* Yield, 90%; m.p. 206–8 °C; IR$_{\nu_{max}}$ (cm^{-1}): 3285 (2NH), 3047 (C–H aromatic), 2922 (C–H aliphatic), 1669 (3 CO); ^{1}H NMR (400 MHz, DMSO-d$_6$): 2.25 (s, 6H, 2CH$_3$), 4.34 (s, 2H, S-CH$_2$), 4.43 (s, 2H, N-CH$_2$), 7.10–8.57 (m, 12H, aromatic protons), 10.29 (s, 1H, NH) (D$_2$O exchangeable), 10.35 (s, 1H, NH) (D$_2$O exchangeable); anal. calcd for $C_{27}H_{24}N_6O_3S$ (512.59): C, 63.27; H, 4.72; N, 16.40. Found: C, 63.01; H, 4.89; N, 16.73.

*4.1.5.5. N-(4-Nitrophenyl)-2-{(5-[2-{(4-nitrophenyl)amino}-2-oxoethyl]-4-oxo-4,5-dihydro-[1,2,4]triazolo[4,3-a]quinoxalin-1-yl)thio}acetamide (**12$_e$**).* Yield, 80%; m.p. 270–2 °C; IR$_{\nu_{max}}$ (cm^{-1}): 3284 (2NH), 3047 (C–H aromatic), 2899 (C–H aliphatic), 1669 (3 CO); ^{1}H NMR (400 MHz, DMSO-d$_6$): 4.39 (s, 2H, S-CH$_2$), 4.49 (s, 2H, N-CH$_2$), 7.60–8.57 (m, 12H, aromatic protons), 10.72 (s, 1H, NH) (D$_2$O exchangeable), 10.81 (s, 1H, NH) (D$_2$O exchangeable); anal. calcd for $C_{25}H_{18}N_8O_7S$ (574.53): C, 52.26; H, 3.16; N, 19.50. Found: C, 52.39; H, 3.44; N, 19.82.

5.1. Docking studies

In the present work, all the target compounds were subjected to docking studies to explore their binding modes towards the DNA active site. All modeling experiments were performed using the Molsoft program, which provides a unique set of tools for the modeling of protein/ligand interactions. It predicts how small, flexible molecules, such as substrates or drug candidates, will bind to a protein of known 3D structure, represented by grid interaction potentials (http://www.molsoft.com/icm_pro.html). Each experiment used the biological target DNA downloaded from the Brookhaven Protein Databank (http://www.rcsb.org/pdb/explore/explore.do?structureId=4G0U). In order to qualify the docking results in terms of the accuracy of the predicted binding conformations in comparison with the experimental procedure, the reported DNA intercalator doxorubicin was used as a reference ligand.

5.2. *In vitro* anti-proliferative activity

The cytotoxicity assays were performed at the Pharmacology & Toxicology Department, Faculty of Pharmacy, Al-Azhar University, Cairo, Egypt. Cancer cells from different cancer cell lines, namely hepatocellular carcinoma (HepG2), colorectal carcinoma (HCT-116) and breast cancer (MCF-7), were purchased from the American Type Cell Culture collection (ATCC, Manassas, USA) and grown on appropriate growth medium (Roswell Park Memorial Institute medium, RPMI 1640) supplemented with 100 mg ml^{-1} of streptomycin, 100 units per ml of penicillin and 10% heat-inactivated fetal bovine serum in a humidified, 5% (v/v) CO_2 atmosphere at 37 °C for the cytotoxicity

assay by 3-[4,5-dimethylthiazole-2-yl]-2,5-diphenyltetrazolium bromide (MTT).

Exponentially growing cells from different cancer cell lines were trypsinized, counted and seeded at the appropriate densities (2000–1000 cells per 0.33 cm^2 well) into 96-well microtiter plates. The cells then were incubated in a humidified atmosphere at 37 °C for 24 hours. Then, the cells were exposed to different concentrations of the compounds (0.1, 10, 100 and 1000 μM) for 72 hours. Then, the viability of the treated cells was determined using the MTT technique as follows. Cells were incubated with 200 μl of 5% MTT solution/well (Sigma Aldrich, MO) and were allowed to metabolize the dye into colored-insoluble formazan crystals for 2 hours. The remaining MTT solution was discarded from the wells, and the formazan crystals were dissolved in 200 μl per well acidified isopropanol for 30 min, covered with aluminum foil and subjected to continuous shaking using a MaxQ 2000 plate shaker (Thermo Fisher Scientific Inc, MI) at room temperature. The colorimetric assay was measured and recorded at an absorbance of 570 nm using a Stat FaxR 4200 plate reader (Awareness Technology, Inc., FL). The cell viability were expressed as the percentage of the control, and the concentration that induces 50% of maximum inhibition of cell proliferation (IC_{50}) was determined using Graph Pad Prism version 5 software (Graph Pad software Inc, CA).[33–35]

5.3. *In vitro* DNA/methyl green assay

The six compounds that exhibited significant anti-proliferative activities (**10_c**, **10_d**, **10_h**, **12_a**, **12_b** and **12_d**) were further evaluated to determine their DNA-binding affinities. Doxorubicin as a DNA intercalator was used as the positive control. In this test, methyl green dye can bind DNA to form a colored reversible complex of DNA/methyl green. These complexes remain stable at neutral pH. Upon addition of intercalating agents, the methyl green is displaced from the DNA with the addition of H_2O molecule to the dye, resulting in the formation of colorless carbinol and leading to a dramatic decrease in the spectrophotometric absorbance.[12,13,36] The ΔA value (the difference between DNA/methyl green complex and free cabinol) provides the simplest means to detect the DNA-binding affinity and relative binding strength. IC_{50} values were determined using Graph Pad Prism 5.0 software. The reaction was performed as follows.

Calf thymus DNA (10 mg) and methyl green (20 mg) (Sigma-Aldrich) were mixed in 100 ml of 0.05 M Tris–HCl buffer (pH 7.5) containing 7.5 mM $MgSO_4$. Then, the mixture was stirred for 24 h at 37 °C. The test samples were dissolved in ethanol and dispensed into wells of a 96-well microtiter tray at concentrations of 10, 100 and 1000 μM. From each well, the excess solvent was removed under vacuum, followed by addition of 200 μl of the DNA/methyl green solution. The test samples were incubated in the dark at ambient temperature. After 24 h, the absorbance of each sample was determined at 642.5–645 nm. The readings were corrected for the initial absorbance and normalized as the percentage of the untreated DNA/methyl green absorbance value.

Conflicts of interest

There are no conflicts to declare.

Acknowledgements

The authors extend their appreciation and thanking to Dr Tamer Abdel-Ghany, Pharmacology & Toxicology Department, Faculty of Pharmacy, Al-Azhar University, Cairo, Egypt for helping in the pharmacological part.

References

1 A. Soni, P. Khurana, T. Singh and B. Jayaram, A DNA intercalation methodology for an efficient prediction of ligand binding pose and energetics, *Bioinformatics*, 2017, **33**(10), 1488–1496, DOI: 10.1093/bioinformatics/btx006.

2 M. F. Braña, M. Cacho, A. Gradillas, B. de Pascual-Teresa and A. Ramos, Intercalators as anticancer drugs, *Curr. Pharm. Des.*, 2001, **7**(17), 1745–1780, DOI: 10.2174/1381612013397113; D. E. Graves and L. M. Velea, Intercalating binding of small molecules to nucleic acids, *Curr. Org. Chem.*, 2000, **4**, 915–929.

3 M. K. Goftar, N. M. Kor and Z. M. Kor, DNA intercalators and using them as anticancer drugs, *Int. J. Adv. Biol. Biomed. Res.*, 2014, **2**(3), 811–822.

4 L. Strekowski and B. Wilson, Noncovalent Interactions With DNA: An Overview, *Mutat. Res.*, 2007, **623**(1–2), 3–13.

5 A. Paul and S. Bhattacharya, Chemistry and biology of DNA-binding small molecules, *Curr. Sci.*, 2012, **102**, 212–231.

6 S. Takenaka and M. Takagi, Threading intercalators as a new DNA structural probe, *Bull. Chem. Soc. Jpn.*, 1999, **72**, 327–337.

7 C. F. Guerra and F. M. Bickelhaupt, WatsonCrick hydrogen bonds: Nature and role in DNA replication, *Modern Methods for Theoretical Physical Chemistry of Biopolymers*, 2006, vol. 19, pp. 79–97.

8 Y. C. Liaw, Y. G. Gao, H. Robinson, G. A. Van der Marel, J. H. Van Boom and A. H. Wang, Antitumor drug nogalamycin binds DNA in both grooves simultaneously: molecular structure of nogalamycin-DNA complex, *Biochemistry*, 1989, **28**, 9913–9918.

9 L. F. Liu, DNA topoisomerase poisons as antitumor drugs, *Annu. Rev. Biochem.*, 1989, **58**, 351–375.

10 A. Chilin, G. Marzaro, C. Marzano, L. Dalla Via, M. G. Ferlin, G. Pastorini and A. Guiotto, Synthesis and antitumor activity of novel amsacrine analogs: the critical role of the acridine moiety in determining their biological activity, *Bioorg. Med. Chem.*, 2009, **17**, 523–529.

11 I. H. Eissa, A. M. Metwaly, A. Belal, A. B. M. Mehany, R. R. Ayyad, K. El-Adl, H. A. Mahdy, M. S. Taghour, K. M. A. El-Gamal, M. E. El-Sawah, S. A. Elmetwally,

M. A. Elhendawy, M. M. Radwan and M. A. ElSohly, Discovery and antiproliferative evaluation of new quinoxalines as potential DNA intercalators and topoisomerase II inhibitors, *Arch. Pharm.*, 2019, **352**(11), e1900123, DOI: 10.1002/ardp.201900123.

12 M. K. Ibrahim, M. S. Taghour and A. M. Metwaly, *et al.*, Design, synthesis, molecular modeling and anti-proliferative evaluation of novel quinoxaline derivatives as potential DNA intercalators and topoisomerase II inhibitors, *Eur. J. Med. Chem.*, 2018, **155**, 117–134, DOI: 10.1016/j.ejmech.2018.06.004.

13 I. H. Eissa, A. M. El-Naggar, N. E. A. A. El-Sattar and A. S. A. Youssef, Design and Discovery of Novel Quinoxaline Derivatives as Dual DNA Intercalators and Topoisomerase II Inhibitors, *Adv. Anticancer Agents Med. Chem.*, 2018, **18**(2), 195–209, DOI: 10.2174/1871520617666170710182405.

14 T. Mahata, A. Kanungo, S. Ganguly, E. K. Modugula, S. Choudhury, S. K. Pal, G. Basu and S. Dutta, The Benzyl Moiety in a Quinoxaline-Based Scaffold Acts as a DNA Intercalation Switch, *Angew. Chem., Int. Ed.*, 2016, **55**, 7733–7736.

15 B. Oyallon, M. Brachet-Botineau, C. Logé, P. Bonnet, M. Souab, T. Robert, S. Ruchaud, S. Bach, P. Berthelot and F. Gouilleux, Structure-based design of novel quinoxaline-2-carboxylic acids and analogues as Pim-1 inhibitors, *Eur. J. Med. Chem.*, 2018, **154**, 101–109.

16 M. G. Varrica, C. Zagni, P. G. Mineo, G. Floresta, G. Monciino, V. Pistarà, A. Abbadessa, A. Nicosia, R. M. Castilho and E. Amata, DNA intercalators based on (1,10-phenanthrolin-2-yl) isoxazolidin-5-yl core with better growth inhibition and selectivity than cisplatin upon head and neck squamous cells carcinoma, *Eur. J. Med. Chem.*, 2018, **143**, 583–590.

17 Y.-S. Park, W.-S. Shin, C.-S. Kim, C. M. Ahn, X.-F. Qi and S.-K. Kim, Molecular and cellular toxicological profiling of DNA bis-intercalator, quinoxaline compounds: echinomycin as the versatile lead, *J. Biochem. Mol. Toxicol.*, 2018, **14**, 9–18.

18 K. El-Adl, H. Sakr, M. Nasser and F. M. A. Shoman, 5-(4-Methoxybenzylidene)thiazolidine-2,4-dione-derived VEGFR-2 inhibitors: Design, synthesis, molecular docking, and anticancer evaluations, *Arch. Pharm.*, 2020, e2000079, DOI: 10.1002/ardp.202000079.

19 E. A. Ahmed, M. F. A. Mohamed, A. Omran and H. Salah, Synthesis, EGFR-TK inhibition and anticancer activity of new quinoxaline derivatives, *Synth. Commun.*, 2020, **50**(19), 2924–2940, DOI: 10.1080/00397911.2020.1787448.

20 M. Alswah, A. H. Bayoumi, K. Elgamal, A. Elmorsy, S. Ihmaid and H. E. A. Ahmed, Design, Synthesis and Cytotoxic Evaluation of Novel Chalcone Derivatives Bearing Triazolo[4,3-*a*]-quinoxaline Moieties as Potent Anticancer Agents with Dual EGFR Kinase and Tubulin Polymerization Inhibitory Effects, *Molecules*, 2017, **23**(1), 48, DOI: 10.3390/molecules23010048.

21 H. G. Ezzat, A. H. Bayoumi and F. F. Sherbiny, *et al.*, Design, synthesis, and molecular docking studies of new [1,2,4]triazolo[4,3-*a*]quinoxaline derivatives as potential A2B receptor antagonists, *Mol. Diversity*, 2020, DOI: 10.1007/s11030-020-10070-w.

22 A. Turky, F. F. Sherbiny, A. H. Bayoumi, H. E. A. Ahmed and H. S. Abulkhair, Novel 1,2,4-triazole derivatives: Design, synthesis, anticancer evaluation, molecular docking, and pharmacokinetic profiling studies, *Arch. Pharm.*, 2020, e2000170, DOI: 10.1002/ardp.202000170.

23 K. El-Adl, A. A. El-Helby, H. Sakr and A. Elwan, Design, synthesis, molecular docking and anti-proliferative evaluations of [1,2,4]triazolo[4,3-a]quinoxaline derivatives as DNA intercalators and Topoisomerase II inhibitors, *Bioorg Chem.*, 2020, **105**, 104399, DOI: 10.1016/j.bioorg.2020.104399.

24 K. El-Adl, A.-G. A. El-Helby, H. Sakr and S. S. A. El-Hddad, Design, synthesis, molecular docking, and anticancer evaluations of 1-benzylquinazoline-2,4(1H,3H)-dione bearing different moieties as VEGFR-2 inhibitors, *Arch. Pharm.*, 2020, e2000068, DOI: 10.1002/ardp.202000068.

25 K. El-Adl, A. A. El-Helby, H. Sakr, I. H. Eissa, S. S. A. El-Hddad and F. M. I. A. Shoman, Design, synthesis, molecular docking and anticancer evaluations of 5-benzylidenethiazolidine-2,4-dione derivatives targeting VEGFR-2 enzyme, *Bioorg. Chem.*, 2020, **102**, 104059, DOI: 10.1016/j.bioorg.2020.104059.

26 A. G. A. El-Helby, *et al.*, Benzoxazole/benzothiazole-derived VEGFR-2 inhibitors: Design, synthesis, molecular docking, and anticancer evaluations., *Arch. Pharm.*, 2019, **352**(12), 1900178.

27 A. G. A. El-Helby, *et al.*, Design, synthesis, molecular docking, and anticancer activity of benzoxazole derivatives as VEGFR-2 inhibitors., *Arch. Pharm.*, 2019, **352**(10), 1900113.

28 A.-G. A. El-Helby, *et al.*, Design, Synthesis, In Vitro Anticancer Activity, ADMET Profile and Molecular Docking of Novel Triazolo [3,4-*a*] phthalazine Derivatives Targeting VEGFR-2 Enzyme, *Anti-Cancer Agents Med. Chem.*, 2018, **18**(8), 1184–1196.

29 S. A. Bailey, D. E. Graves and R. Rill, Binding of actinomycin D to the T (G) nT motif of double-stranded DNA: determination of the guanine requirement in nonclassical, non-GpC binding sites, *Biochemistry*, 1994, **33**, 11493–11500.

30 M. Alswah, A. H. Bayoumi, K. Elgamal, A. Elmorsy, S. Ihmaid and H. E. A. Ahmed, Design, Synthesis and Cytotoxic Evaluation of Novel Chalcone Derivatives Bearing Triazolo[4,3-*a*]-quinoxaline Moieties as Potent Anticancer Agents with Dual EGFR Kinase and Tubulin Polymerization Inhibitory Effects, *Molecules*, 2017, **23**(1), 48–63, DOI: 10.3390/molecules23010048.

31 A. M. Soliman and A. A. Amer, Synthesis and Antimicrobial Activity of Some Novel Quinoxalines, *Synth. Commun.*, 2012, **42**(10), 1401–1410, DOI: 10.1080/00397911.2010.537802.

32 C. C. Wu, T. K. Li and L. Farh, *et al.*, Structural basis of type II topoisomerase inhibition by the anticancer drug etoposide, *Science*, 2011, **333**(6041), 459–462, DOI: 10.1126/science.1204117.

33 T. Mosmann, Rapid colorimetric assay for cellular growth and survival: application to proliferation and cytotoxicity assays, *J. Immunol. Methods*, 1983, **65**(1–2), 55–63.

34 D. A. Scudiero, R. H. Shoemaker, K. D. Paull, A. Monks, S. Tierney, T. H. Nofziger, M. J. Currens, D. Seniff and M. R. Boyd, Evaluation of a soluble tetrazolium/formazan assay for cell growth and drug sensitivity in culture using human and other tumor cell lines, *Cancer Res.*, 1988, **48**(17), 4827–4833.

35 F. M. Freimoser, C. A. Jakob, M. Aebi and U. Tuor, The MTT [3-(4,5-Dimethylthiazol-2-yl)-2,5-Diphenyltetrazolium Bromide] Assay Is a Fast and Reliable Method for Colorimetric Determination of Fungal Cell Densities, *Appl. Environ. Microbiol.*, 1999, **65**(8), 3727–3729.

36 N. S. Burres, A. Frigo, R. R. Rasmussen and J. B. McAlpine, A colorimetric microassay for the detection of agents that interact with DNA, *J. Nat. Prod.*, 1992, **55**, 1582–1587.

37 A. A. El-Helby, R. R. A. Ayyad, M. F. Zayed, H. S. Abulkhair, H. Elkady and K. El-Adl, Design, synthesis, in silico ADMET profile and GABA-A docking of novel phthalazines as potent anticonvulsants, *Arch. Pharm.*, 2019, **352**(5), e1800387, DOI: 10.1002/ardp.201800387.

38 C. A. Lipinski, F. Lombardo, B. W. Dominy and P. J. Feeney, *Adv. Drug Delivery Rev.*, 1997, **23**, 3, DOI: 10.1016/S0169-409X(96)00423-1.

39 D. E. V. Pires, T. L. Blundell and D. B. Ascher, pkCSM, *J. Med. Chem.*, 2015, **58**, 4066, DOI: 10.1021/acs.jmedchem.5b00104.

40 A. Beig, R. Agbaria and A. Dahan, *PLoS One*, 2013, **8**, e68237, DOI: 10.1371/journal.pone.0068237.